NRL Report 6960

Computer Simulation of Structural Details of High-Frequency Over-the-Horizon Earth Backscatter

E. L. Althouse, J. R. Davis, and P. E. V. Shannon

Radar Techniques Branch
Radar Division

November 24, 1969

NAVAL RESEARCH LABORATORY
Washington, D.C.

This document has been approved for public release and sale; its distribution is unlimited.

CONTENTS

Abstract	ii
Problem Status	ii
Authorization	ii
INTRODUCTION	1
THE RAY-TRACE PROGRAMS	1
The NRL Ray-Trace Program	1
The ESSA Ray-Trace Program	2
THE BACKSCATTER SYNTHESIS PROGRAM	4
INTENDED USES OF THE PROGRAMS	10
COMPARISON OF MEASURED AND SIMULATED BACKSCATTER	10
Case 1	10
Case 2	13
Case 3	19
EFFECTS OF ABSORPTION AND ANTENNA PATTERN ON BACKSCATTER	26
SUMMARY AND CONCLUSIONS	33
Comparison of the NRL and ESSA Ray-Trace Programs	33
Antenna Pattern and Absorption	37
Plans for Future Study	38
REFERENCES	38

ABSTRACT

A computer program was developed which simulates high-frequency radar backscatter profiles (giving the amplitude as a function of time delay) from previously computed ray trajectories. The ray trajectories were computed from two different ray-tracing programs; both programs use tabular input descriptions of the antenna pattern and ionospheric electron density profile. One ray-trace program, written at NRL, is a two-dimensional program which generates refraction of the ray trajectories in the ionosphere by applying Snell's law at the boundary of each incremental slab in a uniformly spherically stratified, earth-concentric ionosphere with changing index of refraction. The second, called the ESSA ray-trace program, was written at The Institute for Telecommunication Sciences and Aeronomy, Boulder, Colorado, but was modified at NRL to include the effects of antenna pattern. The ESSA program generates the ray trajectories by performing a three-dimensional, error-checking numerical integration of the six differential Haselgrove equations.

The backscatter profiles which result from the ray trajectories in conjunction with the backscatter synthesis program were compared to actual measured profiles for three cases. The purposes of comparisons between simulated and measured backscatter profiles are: (a) to test the hypothesis that ray trajectories can be predicted reasonably accurately for an HF radar using reduced ionogram data from an appropriately located sounder, (b) to observe the consequences of differences inherent in the two methods of ray tracing, and (c) to investigate the relative validity of various earth backscatter models having dependence on surface roughness and on the elevation angles of the arriving and returning rays.

An analysis was performed for two different model ionospheric electron density profiles to assess the effects of antenna pattern and D-layer absorption on the backscatter profile.

Direct comparison of the ray paths in the three cases studied showed that NRL and ESSA ray traces are usually consistent in group path and ground range within 9%, with the ESSA ray trace predicting longer ray paths in most instances. Good agreement was obtained between the simulated and measured backscatter profiles in two of the three cases for both ray-trace programs, and the hypothesis in (a) was strongly supported.

PROBLEM STATUS

This is an interim report on NRL problem number R02-23. Work is continuing on this and associated phases of the problem.

AUTHORIZATION

NRL Problem R02-23
Projects RF 05-151-402-4007 and MIPR FB 2835-9-916

Manuscript submitted July 10, 1969.

COMPUTER SIMULATION OF STRUCTURAL DETAILS OF HIGH-FREQUENCY OVER-THE-HORIZON EARTH BACKSCATTER

INTRODUCTION

Computer simulation of the propagation of electromagnetic energy provides a simulated controlled-experiment capability in which pertinent variables can be held constant or changed at will. This method holds promise for clarifying the influence of various factors on high-frequency (HF) over-the-horizon radar returns. The effects of (a) antenna pattern, (b) ionospheric absorption and refraction, (c) geomagnetic field, and (d) rough surface scattering on ray trajectories and backscatter returns can be investigated separately. This report describes work at NRL on devising programs to simulate ionospheric earth backscatter and the intended uses of the programs.

The NRL backscatter simulation program can be separated into two basic routines: a ray-trace routine and a backscatter synthesis routine. Presently two ray-trace routines are in use with the backscatter synthesis routine. One ray-trace routine, called the NRL ray trace, was developed at NRL by Harding (1); the other, called the ESSA ray trace, was developed at The Institute for Telecommunication Sciences and Aeronomy (ITSA), Boulder, Colorado, by Jones (2).

THE RAY-TRACE PROGRAMS

The NRL Ray-Trace Program

The NRL ray-trace program is two-dimensional and generates refraction or bending of the ray trajectories in the ionosphere by applying Snell's law at the boundary of each incremental slab in a uniformly spherically stratified, earth-concentric ionosphere with changing index of refraction. Magnetic field and electron collisions are ignored. A quadratic equation is used to interpolate between sliding sets of three points each taken from an ionospheric electron density profile (altitude versus plasma frequency) such that an index of refraction is calculated and stored for every kilometer of height within the ionospheric profile. Caution is necessary to avoid overshoot which occasionally occurs in the interpolation routine. Overshoot occurs when the quadratic equation used to interpolate between a given set of three tabular points acquires a negative slope in some region. Frequently the negative slope occurs between the second and third points of the set and the associated overshoot appears as a long slender parabolic curve connecting the last two points. The consequent local overextension of the ionosphere can produce substantial perturbations on the ray trace. The ionospheric profile is plotted by the computer to allow visual inspection of the quality of the interpolation.

A ray transmitted from the earth's surface at some geographical position continues along a linear trajectory until it reaches the altitude at which appears the first tabulated index of refraction from the electron density profile. Then a connected string of refracted straight line segments are calculated extending until the trajectory turns earthward; this string is reflected about an earth-centered radius vector drawn to the incremental dielectric shell at which the earthward reflection of the ray occurs. The shortcut of defining the downcoming ray as the reflection of the upgoing ray is valid as long as the ray trace is limited to an earth-concentric ionosphere with no magnetic field. Trajectories are calculated for an ensemble of rays evenly spaced in elevation takeoff angle,

terminating with the ray whose equivalent vertical incidence frequency exceeds the maximum plasma frequency (with the ray that first penetrates the ionosphere). The antenna pattern is imposed on the ray plot by suppressing appropriate ones of the evenly spaced rays in elevation angle so as to approximate a spacing of rays that is in inverse proportion to the power density radiated. This provides a visual aid for locating spacial regions of high power density. The group path length, ground range, and power radiated are calculated and stored for each ray. Since the intrastratum medium is taken as isotropic, the ray vector and wave normal are coincident, thereby allowing the group path length of each segment to be determined by multiplying the geometrical length of the segment by the group refractive index; this parameter, consistent with earlier restrictions, is equal to the reciprocal of the phase refractive index.

The antenna pattern can be determined from a combination of the elevation and azimuthal plane patterns. Since the ray trace is two-dimensional, with the rays lying in a vertical plane along the beam-centered azimuth, only the integral of the azimuthal gain pattern is of importance. The results of this integral for six different carrier frequencies from 10 to 30 MHz are used in an interpolation routine which calculates the correct integrated azimuthal gain for a desired operation frequency. For convenience the azimuthal pattern is assumed independent of elevation angle; departures from this assumption are accounted for by adjusting the appropriate vertical gain factors. The vertical gain pattern from 0 to 30 degrees elevation at any operating frequency is calculated from a weighted average of three input patterns measured at three different frequencies. The interpolation expression is

$$G = \left(G_1 |\lambda_0 - \lambda_1|^{-1} + G_2 |\lambda_0 - \lambda_2|^{-1} + G_3 |\lambda_0 - \lambda_3|^{-1} \right) / \left(|\lambda_0 - \lambda_1|^{-1} + |\lambda_0 - \lambda_2|^{-1} + |\lambda_0 - \lambda_s|^{-1} \right) ,$$

where G_i $(i = 1, 2, 3)$ is the gain for a particular elevation, λ_0 is the wavelength at the operation frequency and λ_i $(i = 1, 2, 3)$ is the wavelength at the frequency for which the collection of measured antenna parameters (G_i) are provided. In the event $\lambda_0 = \lambda_i$, the interpolation is bypassed and the appropriate measured pattern is used. If the vertical pattern is sensitive to the azimuthal aspect of the antenna, the three input vertical patterns must be measured at the appropriate azimuth.

All of the ray-trace illustrations in this report have the vertical scales doubled to enhance details in the illumination patterns. The vertical scale is doubled in a polar coordinate system by doubling the difference between the length of the radius vector to a given ray point and the earth's radius, adding this to the earth's radius, and then finding the cartesian components of the resultant vector. An unfortunate consequence of the expansion is a distortion frequently manifested as an upward bend in a ray trajectory. This behavior is most apparent in ray traces shown near the end of the report and should be recognized as a distortion only on the illustration and not in the calculations.

Figure 1 shows a ray trace with antenna pattern generated from the ionospheric profile shown in Fig. 2. Three major antenna lobes are clearly recognizable from the variation in ray density.

The ESSA Ray-Trace Program

The ESSA ray-trace program performs a three-dimensional, error-checking numerical integration of the six differential Haselgrove equations (3). A detailed description of this program is given in Ref. 2. In contrast to the simpler NRL ray-trace program, the

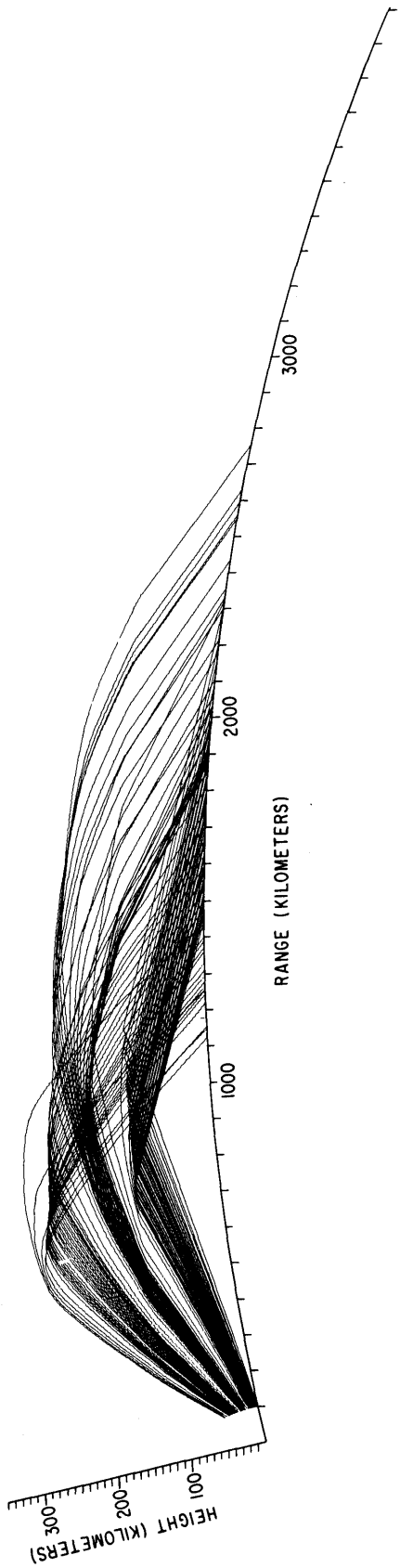

Fig. 1 - NRL ray trace (Case 1)

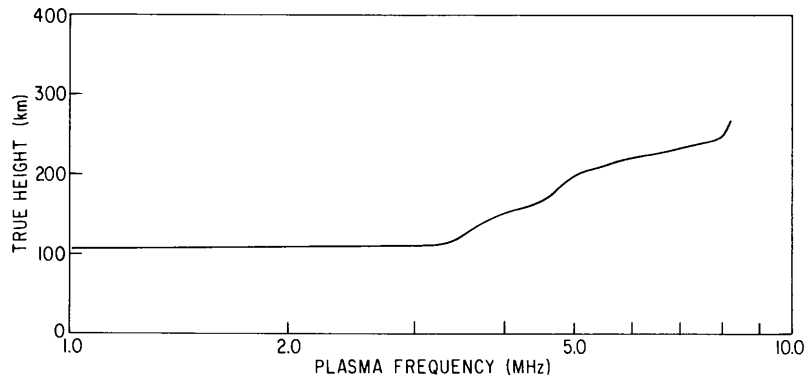

Fig. 2 - Measured ionospheric profile (Case 1)

ESSA program can treat the effects of magnetic field, electron collisions, and nonconcentric ionospheres. The programmer has the option of plotting either the ordinary or extraordinary ray in an arbitrarily oriented vertical or horizontal plane. The amount of error tolerable in the numerical integrations can be specified so as to produce highly accurate (and hence expensive) or less accurate (and inexpensive) ray traces. Ionospheric profiles are fed in either by a table of true height versus plasma frequency or by a selection between linear, parabolic, and Chapman analytic models. Two routines are also available to add perturbations to the analytic models. The true-height table is interpolated by a sophisticated quadratic and cubic curve fitting technique which forces continuity of the first derivative of the resultant ionospheric profile. Initially a quadratic is fitted to three adjacent points in the profile, and, from this quadratic, the gradient is determined at the middle point. A cubic is then fitted between each two adjacent points in the profile. The coefficients are chosen so that the cubic matches the value of the profile and its gradient at each of these two points. Since the ESSA ray-trace program is being used with a two-dimensional backscatter synthesis, its three-dimensional capability is not presently being utilized.

An NRL modification to this ray-trace program permits the inclusion of antenna pattern effects by varying the ray takeoff angles in inverse proportion to the radiated power density. As before, a two-dimensional antenna pattern is used. A segmented least-square polynomial fit is made to the vertical antenna pattern for a fixed frequency and azimuth, and the resulting set of polynomial coefficients for each segment is fed in to the ESSA program. The coefficients are then used in an analytical integration of the antenna pattern over elevation angle to define ray takeoff angles such that each ray carries the same amount of energy. The antenna pattern appears in the ray plots by the variation in angular separation between rays. An ESSA ray trace is shown in Fig. 3 for the same ionospheric profile as shown in Fig. 2. The last ten rays are terminated because they penetrated the ionosphere. The general features of both ray traces are very similar; however, the NRL ray trace predicts a 4% shorter minimum ground range. The maximum ground range of the NRL ray trace was 3232 km, but the associated ray was not shown because of the plotting scheme used to show the antenna pattern. A larger overall ray density was used for the ESSA ray trace. The minor differences between Figs. 1 and 3 are attributed to the two different approaches of calculating the ray trajectories.

THE BACKSCATTER SYNTHESIS PROGRAM

In essence the backscatter synthesis program repropagates the earth-scattered energy from incremental areas of the illuminated region along all possible tubular paths to

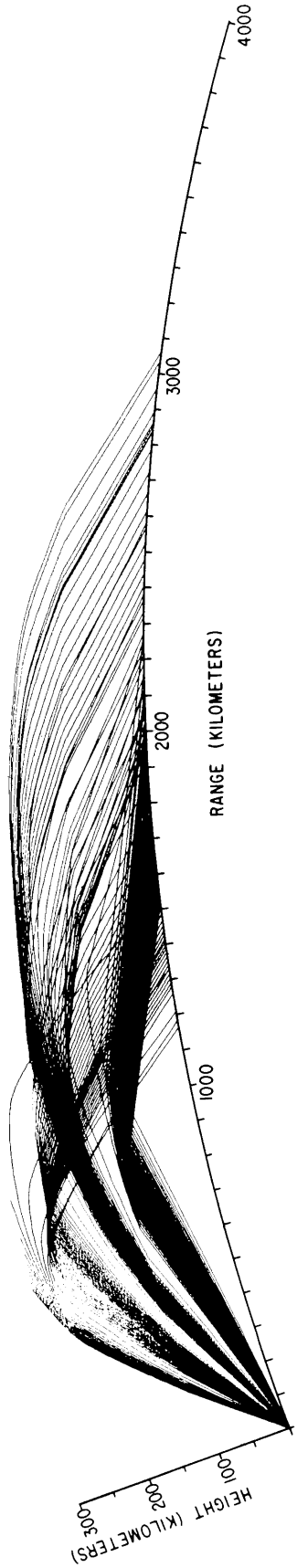

Fig. 3 - ESSA ray trace (Case 1)

the receiver, using the same ray path geometry as was generated in the original ray trace. The following discussion briefly describes the logic of this program. A more detailed description of an earlier version is given in Ref. 1.

An increment of energy transmitted from the radar antenna (used both for transmitting and receiving) is assumed to follow a tubular trajectory defined by adjacent ray paths. The fraction of the total energy emitted in a radar pulse which is carried by a given tube is determined by this tube's initial angular spread and the antenna gain corresponding to its elevation takeoff angle. This energy, minus losses, is assumed to be uniformly distributed over the ground surface illuminated by that tube. As illustrated in Fig. 4, ionospheric focusing causes some tubes to overlap in ground range, allowing the earth-scattered energy in the overlap region to return to the antenna through several alternative tubes or modes. This illustration shows four rays adjacent in elevation angle. Outgoing energy in tube 3-4 can return in tubes 1-2, 2-3, and 3-4. The amount of energy considered available for return by an alternate mode is determined as follows. The incident energy of a given mode is first reduced by an amount dictated by the assumed earth backscattering characteristics for the incidence angles of the arrival and return flux tubes. This quantity is then reduced once more by a factor equal to the ratio between the range interval on the earth common to both tubes and the range interval on the earth within the arrival tube. For example,

$$E_{12} = G_{12}^{34} E'_{34} \frac{R_1 - R_2}{R_4 - R_s} ,$$

where E_{12} is the energy returning through tube 1-2, E'_{34} is the energy arriving on the ground through tube 3-4, R_i $(i = 1, 2, 3, 4)$ is the ground range of ray i, and G_{12}^{34} is a backscatter factor which depends on the angles of the four rays and the roughness properties of the surface. For return by the same tube or mode, the incident energy is modified only by the backscatter model. The energy delivered to the receiver along a given return tube is further adjusted by the ratio of the effective antenna aperture at the returning angle to the cross-sectional area of that tube when it arrives at the receiving antenna.* An empirical expression determined by Lucas and Haydon (4) is used to introduce an absorption factor to correct for energy losses incurred in propagation through the D region of the ionosphere, which is assumed to begin at 75 km altitude. The

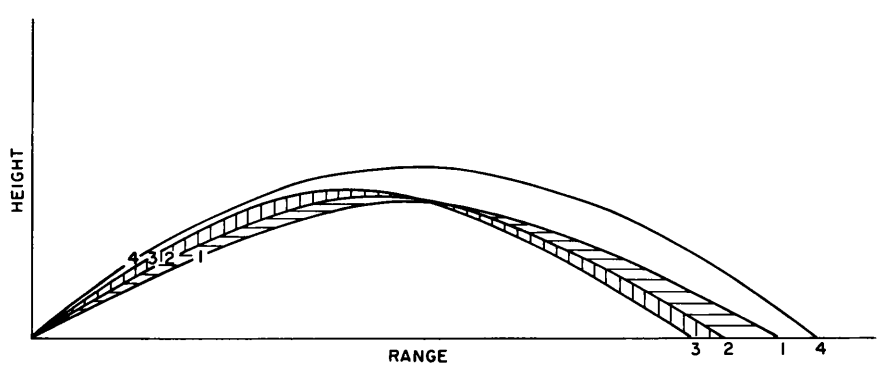

Fig. 4 - Ionospheric focusing

*Here it is assumed that the return tube actually emanates from a point on the earth and spreads as it approaches the receiving antenna.

necessary input variables for the absorption calculation are the solar zenith angle, the gyromagnetic frequency at 100 km, the sunspot number (the predicted number of sunspots for the given month), and the average angle of incidence of the tube with the D layer.

For each possible combination of outgoing and return tubes, the maximum and minimum propagation times are calculated from the group paths; the difference between these propagation times ΔT is used to calculate the power delivered by that mode: $P_{del} = E_{del}/\Delta T$, where E_{del} is that portion of the originally transmitted incremental energy which is returned by the mode under consideration. Initially it is assumed that an incremental rectangular pulse of width ε is transmitted. A time base is constructed of successive increments, each of length ε, such that a time T_n is specified by naming the increment (i.e., $T_n = n\varepsilon$). The total energy E_{del} delivered by a particular mode at some mean time T_m over a time span of ΔT is appropriately stored in elements of a power array P_n as indicated below.

$$\sum_{n=N}^{N'} P_n \, n\varepsilon = P_{del} \, \Delta T = E_{del} \, , \tag{1}$$

where

$$(N' - N)\,\varepsilon \approx \Delta T$$

$$(N' + N)\,\varepsilon/2 \approx T_m \, .$$

Since $(N' - N)\varepsilon$ can take on only discrete values, while ΔT can take on any value, in general $(N' - N)\varepsilon$ does not identically equal ΔT. In this case N' and N are chosen such that $(N' - N)\,\varepsilon > \Delta T$ and $P_{N'}$ and P_N are adjusted so as to satisfy energy conservation. The time-indexed power array P_n is cumulatively filled with the contributions of all the return modes. The artificiality of assuming an incremental rectangular pulse is removed by generating the actual (usually sine-squared) radar pulse by appropriately amplitude-modulating and time-sequencing a finite sum of contiguous rectangular pulses of width ε. Mathematically, this convolution process is achieved by the summation expression

$$P'(M) = \sum_{L=1}^{L'} P(M - L + 1) \, \sin^4 \left[(L - 0.5) \, \frac{\varepsilon\pi}{\tau} \right] , \tag{2}$$

where P' is the power returned in the mth time interval from the sine-squared pulse of width τ, P is the power returned in the $(M - L + 1)$th time interval from the original incremental pulse, and L' is the number of contiguous incremental pulses used to generate the sine-squared pulse.

The angular variation of the diffuse portion of the earth-scattered energy (the backscatter pattern) can be calculated from the results of Beckmann (5), who evaluated the Helmholtz integral as a solution of the wave equation using the usual Kirchhoff approximation of the boundary conditions:

1. The dimensions of the scattering surface are assumed to be much greater than the wavelength of the incident radiation.

2. The radius of curvature of the scattering elements is taken to be much greater than the wavelength of the incident radiation.

3. Shadowing effects are neglected.

4. Only the far field is calculated.

5. Multiple scattering is neglected.

A two-dimensional model of surface roughness, defined by a statistical Gaussian distribution of surface heights

$$w(z) = \frac{1}{\sigma\sqrt{2\pi}} e^{-z^2/2\sigma^2} \tag{3}$$

and a correlation of the density of irregularities given by

$$C(\tau) = e^{-\tau^2/T^2} , \tag{4}$$

is used to describe the scattering boundary. In Eq. (3), σ is the standard deviation of surface heights, which are assumed to have a mean value of zero, and in Eq. (4), τ is a separation parameter defined as

$$\tau = x_1 - x_2 ,$$

where x_i is one coordinate of the point at which the surface height $z = z(x_i, y_i)$ is measured, and T is the correlation distance for which $C(\tau)$ drops to the value $1/e$. A rough surface is not completely specified by a statistical distribution of surface heights alone. Some information must be available about the distances between hills and valleys of the surface, and this is contained in the normalized correlation function $C(\tau)$ which may be expressed generally as

$$C(\tau) = \frac{\langle z_1 z_2 \rangle - \langle z_1 \rangle \langle z_2 \rangle}{\langle z_1^2 \rangle \langle z_1 \rangle^2} , \tag{5}$$

where z_1 and z_2 are surface heights at two arbitrary points, and where

$$\langle z_1 z_2 \rangle = \lim_{L \to \infty} \frac{1}{2L} \int_{-L}^{L} z(x)\, z(x+\tau)\, dx . \tag{6}$$

For a mean surface height of zero, Eq. (5) reduces to

$$C(\tau) = \frac{\langle z_1 z_2 \rangle}{\langle z_1^2 \rangle} .$$

For a purely random surface,

$$\lim_{\tau \to 0} C(\tau) = 1$$

and

$$\lim_{\tau \to \infty} C(\tau) = 0 ,$$

provided the surface contains no nonrandom periodic components. Beckmann uses Eq. (4) as a sufficiently general form of the correlation function satisfying the last three equations. Since the roughness of the scattering surface modifies the scattered field far more

than its electrical properties, Beckmann simplifies the calculation by assuming perfect electrical conductivity. The crosspolarized component of the scattered field is ignored. Beckmann's expression for the scattering coefficient is in the form of an infinite series, which for a very slightly rough surface simplifies to

$$\langle \rho\rho^* \rangle = e^{-g} \left(\rho_0^2 + \frac{g\pi T^2 F}{A} e^{-v_{xy}^2 T^2/4} \right), \tag{7}$$

and for a very rough surface simplifies to

$$\langle \rho\rho^* \rangle = \frac{\pi F^2 T^2}{A v_z^2 \sigma^2} e^{-\left(\frac{v_{xy}^2 T^2}{4 v_z^2 \sigma^2} \right)} \tag{8}$$

In these equations

$$F = \frac{1 + \cos\theta_1 \cos\theta_2 - \sin\theta_1 \sin\theta_2 \cos\theta_3}{\cos\theta_1 (\cos\theta_1 + \cos\theta_2)},$$

in which θ_1 is the angle of incidence with respect to the overall surface normal, θ_2 is the scattering angle with respect to this normal, and θ_3 is a lateral scattering angle. Also in these equations

$$v_{xy} = \frac{2\pi}{\lambda} [\sin^2\theta_1 - 2 \sin\theta_1 \sin\theta_2 \cos\theta_3 + \sin^2\theta_2]^{1/2},$$

$$v_z = \frac{2\pi}{\lambda} (\cos\theta_1 + \cos\theta_2),$$

in which λ is the radar wavelength, and

$$g = v_z^2 \sigma^2$$

Further, A is the surface area illuminated and ρ_0 is the specular reflection term (which does not contribute in backscatter work). For the moderately rough surface there appears to be no simplified expression except in the specular direction. Presently the backscatter synthesis program uses the two simplified expressions as well as an isotropic model either singly or in combination to generate a backscatter pattern (scattering coefficient versus return angle θ_2) for each energy tube incident at angle θ_1. Ignoring lateral variations of θ_3, the integral I_1 of the backscatter pattern over θ_2 from $-\pi/2$ to $\pi/2$ is assumed to be proportional to the energy of the arrival tube under consideration. The effect of the backscatter pattern on returning energy is given as a multiplicative ratio of the integral of the pattern over the angular spread of the return tube (θ_2 to $\theta_2 + \Delta\theta_2$) to the integral I_1. The above integrations are carried out numerically using a CDC cooperative computer library subroutine identified as D1 Sand Gaussn.

This program plots the predicted power or voltage or both versus time delay.* If calculations are made for more than one backscatter model or for a combination of models (say X% isotropic, 100 - X% nonisotropic), the corresponding voltage and power plots

*Time delay is used here as the amount of elapsed time between transmission of the pulse and reception of the backscattered signal.

are superimposed and labeled for visual comparison. A plot of experimentally observed voltage versus time delay can also be superimposed, if desired, to demonstrate the degree of agreement between simulation and actual experiment.

INTENDED USES OF THE PROGRAMS

The backscatter simulation program was originally written to test the hypothesis that ray trajectories can be predicted reasonably accurately for an HF radar using reduced ionogram data from an appropriately located sounder (say at midpath along the transmission azimuth). A favorable comparison of the simulated backscatter with that actually measured (time-exposed photograph) under the same conditions will strongly support the accuracy of this hypothesis. A good fit is evidence that the ray paths and any other calculations based on them are correct. A major portion of the next section of this report indicates the degree to which predicted backscatter matches experimental backscatter. Photographs of backscatter returns are usually exposed for 10 seconds in an effort to average out amplitude variations caused by short-term ionospheric electron-density fluctuations.

Judging the accuracy of a given set of rays by the backscatter matching technique is complicated by the fact that the backscatter amplitude structure depends also on the nature of the scattering surface (its roughness and associated statistical properties), on absorption incurred during transit through the *D* layer, and on tilts or horizontal gradients in the ionospheric electron density. Thus the program is also being used to investigate the relative validity of various backscatter models having dependence both on surface roughness and on the elevation angles of the returning rays and to investigate *D*-layer absorption models. The investigation of the effects of ionospheric tilts will require additions to the present program.

COMPARISON OF MEASURED AND SIMULATED BACKSCATTER

Case 1

Figure 5 is a photograph of backscatter in a voltage-vs-time-delay format taken at the NRL HF radar field site on May 25, 1964. The pertinent data for analysis are as follows:

Time,	1925 GMT;
Transmitter frequency,	15.595 MHz;
Azimuth,	192 deg;
Pulse length,	700 μsec;
Sunspot number,	11.0;
Solar Greenwich hour angle,	109.54 deg;
Solar declination,	+21.058 deg.

Calibration markers appear at multiples of 5.556 milliseconds and should not be interpreted as part of the backscatter. The very jagged structure of the return is due to amplitude fluctuations mentioned earlier. Time exposures of the backscatter of about 10 seconds duration usually give consistent results, with most short-term fading removed. The envelope of the photograph in Fig. 5 was scaled on an x-y reader to permit plotting

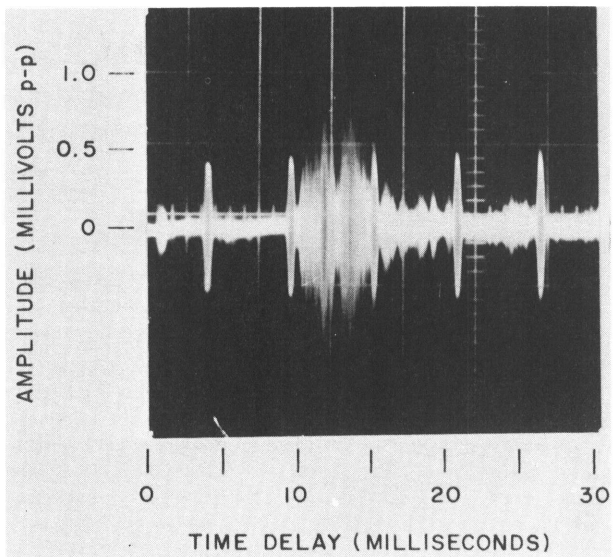

Fig. 5 - Observed backscatter (Case 1). Five calibration markers appear which are not part of the backscatter.

of the data directly over the simulated backscatter. Figure 2 shows a true-height-vs-plasma-frequency ionospheric profile as measured and reduced by the San Salvador sounder station at 1859 GMT of the same day. This ionospheric profile displays the presence of E, F_1, and F_2 layers. The NRL ray trace corresponding to this ionospheric profile was shown in Fig. 1, in which rays reflected from each of these layers may be discerned. The ground coverage is approximately 1120 km to 2750 km, which at an azimuth of 192 degrees corresponds to coverage from Jacksonville, Florida, to the eastern tip of Honduras. San Salvador lies approximately in the middle of the ground and water coverage but approximately 600 naut mi east of the 192-degree azimuth from Washington, D.C. The three portions of the plasma frequency profile corresponding to steep electron density gradients appear as regions of strong refraction in the ray trace at the altitudes of the three layers mentioned.

The predicted distribution of the received earth backscatter signal generated from this ray trace for an isotropic earth-scatter model is shown as a solid curve in Fig. 6 along with an approximate scaling of Fig. 5 (dashed curve) for comparison. The beginning and ending of the computed profile (8.6 and 22.0 msec respectively) correspond to the rays with minimum and maximum group path; in this case these rays also have the minimum and maximum ground range respectively. The leading edge of the simulated profile occurs 1.6 msec too early. The leading edge of the second major peak (13.2 msec) is in excellent agreement; however, its trailing edge drops off about 0.6 msec too early. The location and relative amplitude at the major null at 13 msec is in excellent agreement. It is encouraging that the general features of both profiles are similar.

A second backscatter profile, shown in Fig. 7, was computed for the same ray trace using the "very rough surface" Beckmann (VRB) earth-scatter formulation (see Eq. (8)) with a roughness parameter of $2\sigma/T = 15.0$. The beginning and ending times of the profile are the same as before, but the initial steep rise of the profile is suppressed until later time delays, resulting in a better "early fit." The amplitude of the null at 13 msec and of the tail between 14 and 16.5 has increased. The trailing edge of the second major peak still drops off about 0.6 msec too early.

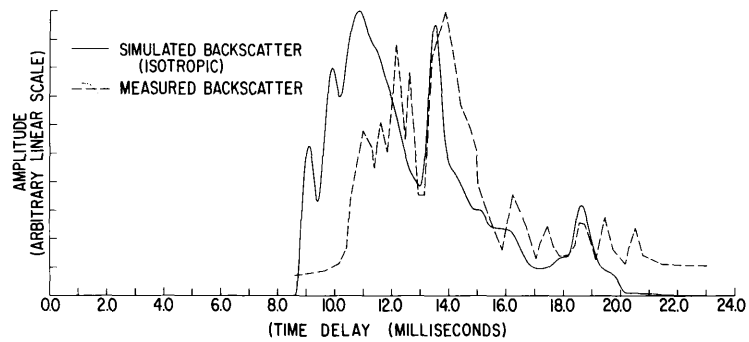

Fig. 6 - Backscatter comparison using the NRL ray trace and the isotropic earth-scatter model (Case 1). The ground range is obtained by the conversion 1 msec ≈ 150 km.

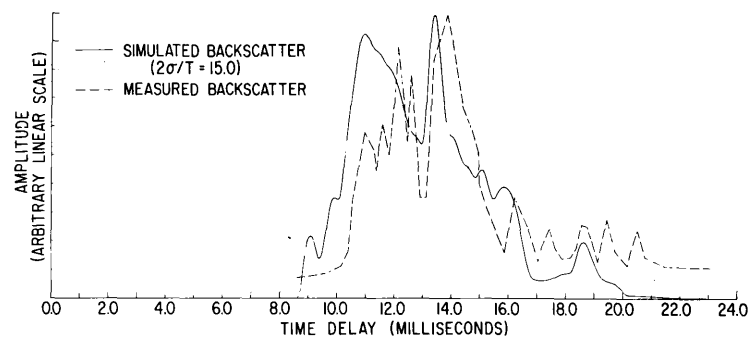

Fig. 7 - Backscatter comparison using the NRL ray trace and the VRB (very rough — Beckmann) earth-scatter model (Case 1). The ground range is obtained by the conversion 1 msec ≈ 150 km.

The corresponding ESSA ray trace is shown in Fig. 3. The appearance of slightly longer range rays than present in the NRL ray trace occurs because some of the NRL rays were suppressed in representing the antenna pattern. (The NRL ray trace actually generated rays having up to 3232 km ground range.) The ten incomplete ray paths at high takeoff angles in Fig. 3 are rays that penetrate the ionosphere. In subsequent ray traces the plotting routine was set to ignore all rays at angles higher than that of the first ray to penetrate.

The tightly grouped *E*-layer rays start at about 1510 km ground range for the ESSA ray trace and at about 1450 km for the NRL ray trace. The two-way time delay for this ray group is from 9 to 15 msec. A shift of the computed backscatter profile for the ESSA ray trace toward later time delays with respect to those computed from the NRL trace would be expected. This shift is observed, as seen in Fig. 8. Relative to Fig. 6 the initial rise of the profile as well as the position of the second major peak is significantly delayed. The position of the null around 13 msec is still good; however, the new bump at 15.5 msec is absent in the measured data. A second backscatter profile shown in Fig. 9 was computed using the VRB earth-scatter formulation with a roughness parameter of 15.0. Although the initial profile rise now agrees well with that measured, the amplitudes of the null at 13 msec and the unwanted peak at 15.5 msec are raised, resulting in a poorer fit at the longer time delays.

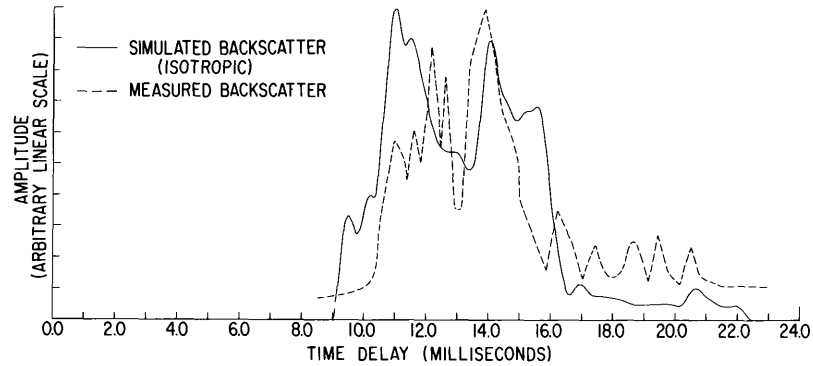

Fig. 8 - Backscatter comparison using the ESSA ray trace and the isotropic earth-scatter model (Case 1). The ground range is obtained by the conversion 1 msec ≈ 150 km.

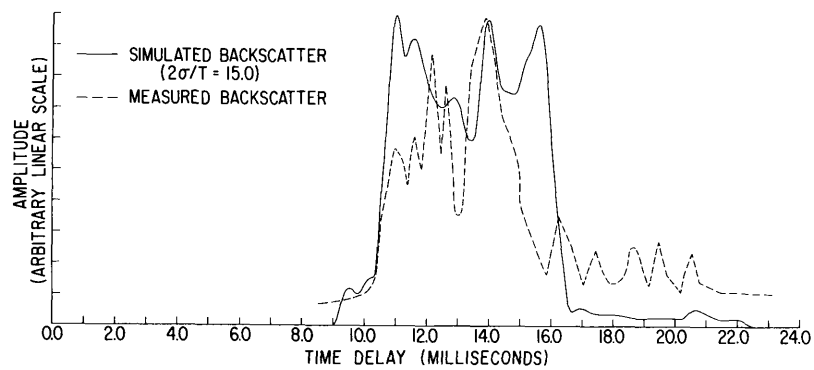

Fig. 9 - Backscatter comparison using the ESSA ray trace and the VRB earth-scatter model (Case 1). The ground range is obtained by the conversion 1 msec ≈ 150 km.

The leading edge of the profiles simulated from the ESSA ray trace is in better agreement with the leading edge of the measured profile than are those simulated from the NRL ray trace. The position of the major null and the leading edge of the second major peak are best simulated by the NRL ray trace. The trailing edge of the NRL simulated profile is qualitatively correct, but it occurs 0.6 msec prematurely. The trailing edge of the ESSA simulated profile has additional structure not present in the measured profiles.

The VRB earth scatter model improved the agreement in position of the leading edge between simulated and measured profiles for both ray traces; however, the isotropic earth-scatter model improves the agreement between relative amplitudes of the null at 13 msec. The isotropic model also seems to give a more realistic trailing edge to the ESSA simulated profile.

Case 2

Backscatter observed on May 25, 1964, is shown in Fig. 10. Calibration markers again appear at multiples of 5.556 msec. The data required for analysis are as follows:

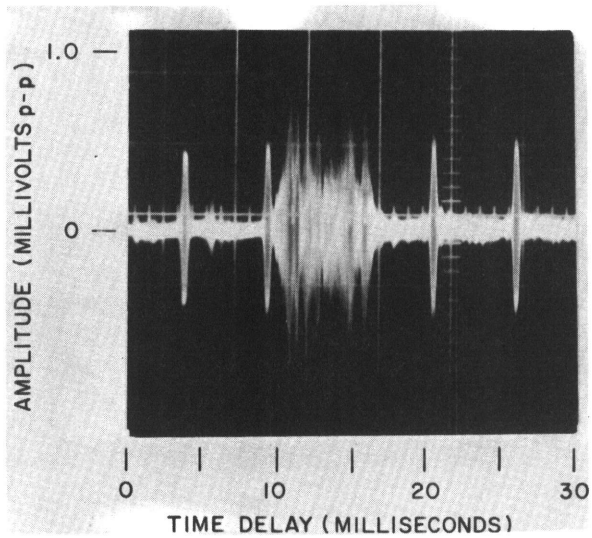

Fig. 10 - Observed backscatter (Case 2)

Time,	1840 GMT;
Transmitter frequency,	15.595 MHz;
Azimuth,	192 deg;
Pulse length,	700 μsec;
Sunspot number,	11.0;
Solar Greenwich hour angle,	98.28 deg;
Solar declination,	+21.05 deg.

A true-height-vs-plasma-frequency ionospheric profile is shown in Fig. 11 as measured and reduced by the Cape Kennedy sounder station at 1829 GMT of the same day. The NRL ray trace corresponding to these ionospheric conditions is shown in Fig. 12. This time there are only two regions of intense refraction, occurring around 110 and 215 km,

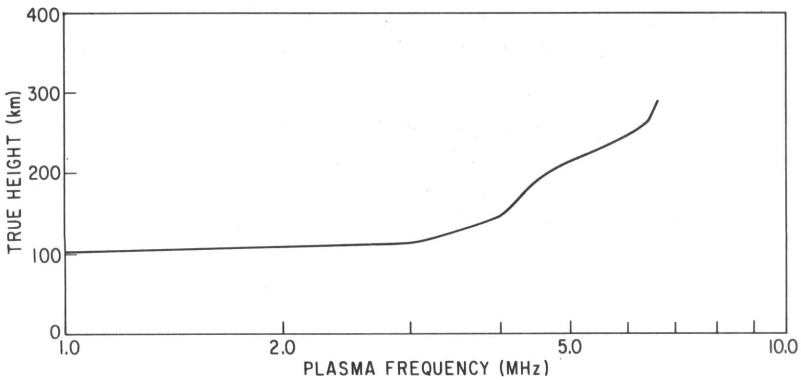

Fig. 11 - Measured ionospheric profile (Case 2)

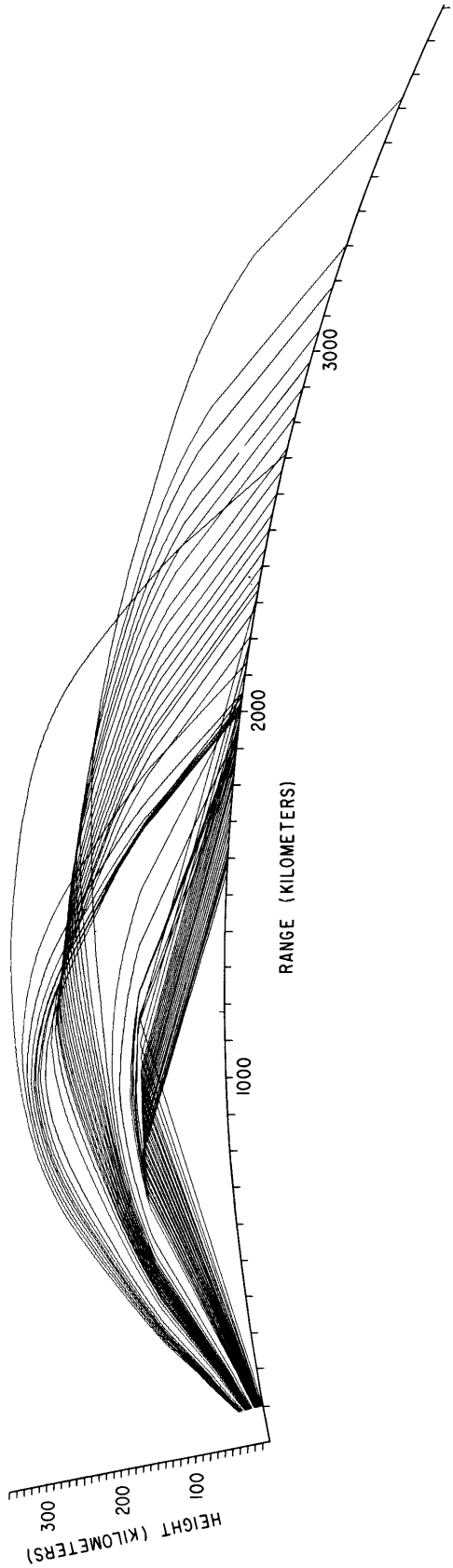

Fig. 12 - NRL ray trace (Case 2)

an *E* layer and a single *F* layer. The minimum and maximum two-way time delays for this ray set are 10.6 and 31.0 msec, respectively, corresponding again to minimum and maximum ground ranges of 1562 and 4410 km. As before, the longest-range ray was not plotted. Along a 192-degree azimuth the terrain illumination extends approximately from the southern tip of Florida to the equator; however, the most intensely illuminated area lies from 1562 km to 2050 km or from the southern tip of Florida to about 110 naut mi beyond Cuba, corresponding to two-way time delays between 10.6 and 15.1 msec.

The backscatter profile generated from this ray trace for an isotropic earth-scatter model is shown as a solid curve in Fig. 13, along with an approximate scaling of Fig. 10 (dashed curve) for comparison. The leading edge of the computed profile at 10.6 msec is in good agreement with that of the measured profile, but there is a large discrepancy between relative amplitudes. The measured null at 13.6 msec appears shifted toward the right in the computed curve, whereas the measured peak at 15.4 msec appears shifted toward the left. The measured peak at 16.5 msec does not appear in the computed curve, and the tails from 17.5 msec to 24 msec are not in good agreement. A second backscatter profile shown in Fig. 14, was computed for the same ray trace using a roughness parameter of 15. Here the overall fit to the measured curve is substantially better than in Fig. 13. The relative amplitudes in the region from 11 to 14 msec are in better agreement, and a new peak appears at 16 msec, suggestive of the much larger measured peak at 16.5 msec. The structure of the tail from 17.5 to 24 msec remains almost unchanged.

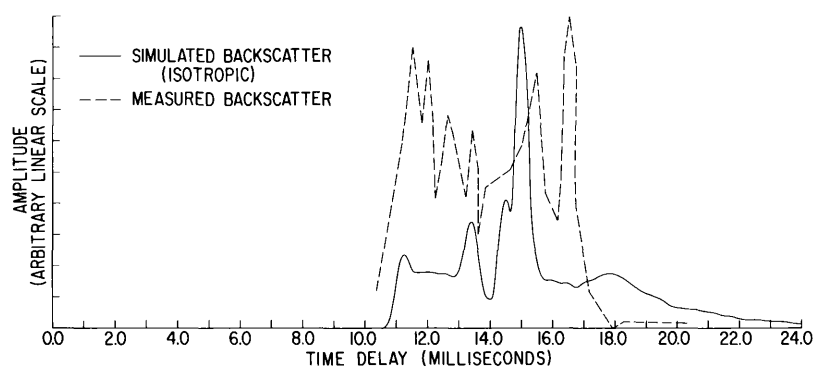

Fig. 13 - Backscatter comparison using the NRL ray trace and the isotropic earth-scatter model (Case 2). The ground range is obtained by the conversion 1 msec ≈ 150 km.

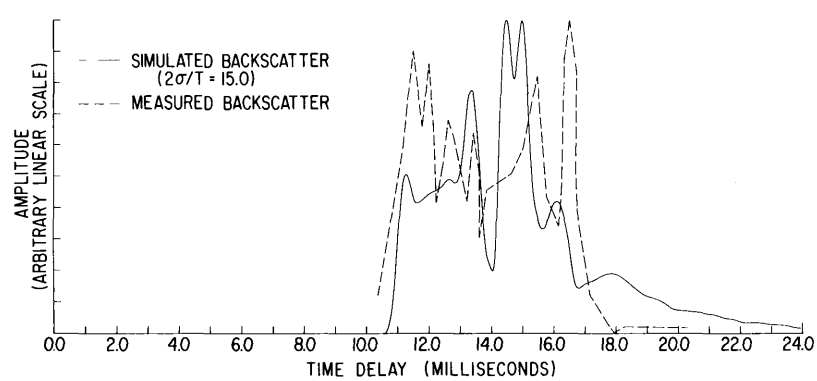

Fig. 14 - Backscatter comparison using the NRL ray trace and the VRB earth-scatter model (Case 2). The ground range is obtained by the conversion 1 msec ≈ 150 km.

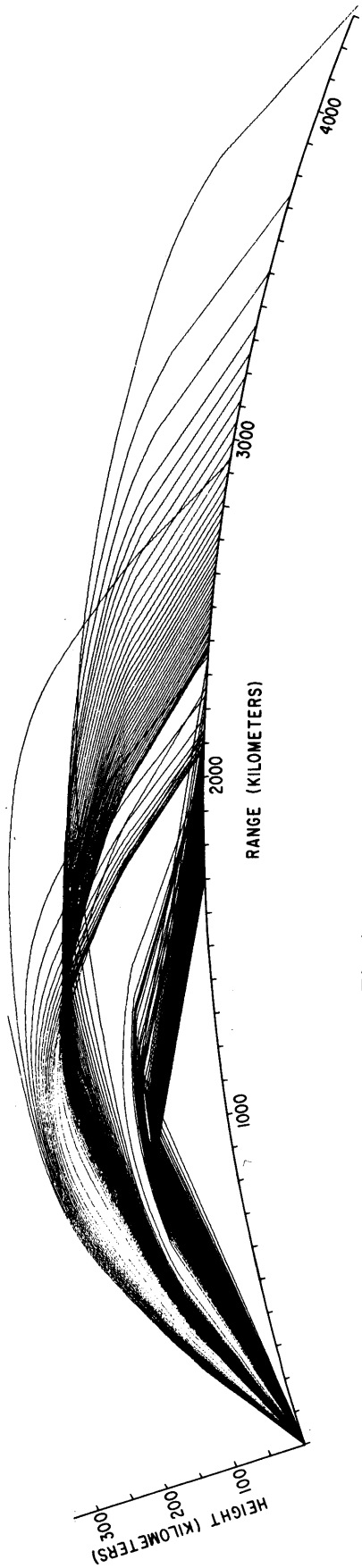

Fig. 15 - ESSA ray trace (Case 2)

The corresponding ESSA ray trace is shown in Fig. 15. Note that the shortest ground range (1690 km) is somewhat longer than predicted by the NRL ray trace. The most intensely illuminated region falls between ground ranges of 1700 km and 2140 km, corresponding to two-way delay times between 11.6 and 15.7 msec. Another moderately intensely illuminated region lies between ground ranges of 2340 km and 3000 km, corresponding to two-way delay times from 16.8 to 21.2 msec; this region is probably responsible for the tail of the computed isotropic backscatter profile shown in Fig. 16. The effect of the longer-range low-angle rays in the ESSA calculation, relative to the NRL version, is a delayed appearance of the beginning of the computed profile. With the exception of the peak at 14.1 msec, the relative amplitudes of the curves are in better agreement than they were for the NRL isotropic profile.

The backscatter profile computed for a roughness parameter of 15.0 is shown in Fig. 17. A new minor peak has formed at 16.5 msec. It is speculated that had other roughness parameters been tried, the amplitude of this peak could have been pushed up to obtain better agreement with the measured curve — at least at later time delays. It is encouraging that many of the profile peaks occur at nearly the same time delay as that of the peaks of the measured curve, even though the relative amplitudes are frequently not in close agreement.

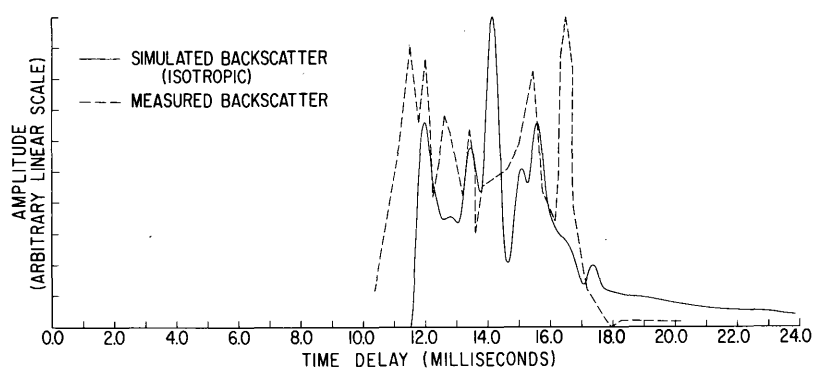

Fig. 16 - Backscatter comparison using the ESSA ray trace and the isotropic earth-scatter model (Case 2). The ground range is obtained by the conversion 1 msec ≈ 150 km.

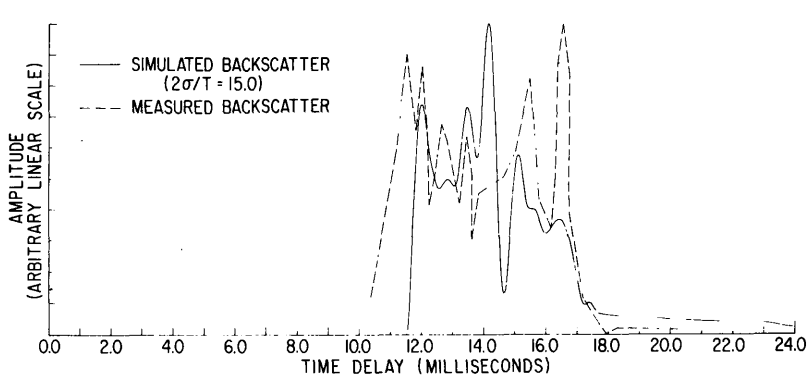

Fig. 17 - Backscatter comparison using the ESSA ray trace and the VRB earth-scatter model (Case 2). The ground range is obtained by the conversion 1 msec ≈ 150 km.

The leading edges of the NRL simulated profiles are in better agreement with the measured profile than are those of the ESSA simulated profiles. This is just the opposite circumstance from that observed in Case 1. The trailing edges are, however, in better agreement in the ESSA simulated profiles. For the isotropic scatter model the best agreement between the measured and simulated amplitude structure was obtained with the ESSA ray trace. For both ray traces, the backscatter profiles generated using the VRB scatter model were in better overall agreement with those measured.

Case 3

Backscatter observed on July 30, 1964, is shown in Fig. 18, with calibration markers again appearing at multiples of 5.556 msec. The data required for analysis are as follows:

Time,	1550 GMT;
Transmitter frequency,	18.036 MHz;
Azimuth,	192 deg;
Pulse length,	700 μsec;
Sunspot number,	0.0;
Solar Greenwich hour angle,	65.92 deg;
Solar declination,	+18.40 deg.

A true-height-vs-plasma-frequency ionospheric profile is shown in Fig. 19 as measured and reduced by the Grand Bahama sounder station at 1630 GMT of the same day. The ionogram suggests that there is only one region of intense refraction (an E layer), and this is indeed the case, as seen in the NRL ray trace in Fig. 20. The span of the plotted rays is from 1690 km to 2320 km, corresponding to time delays from 11.4 msec to about

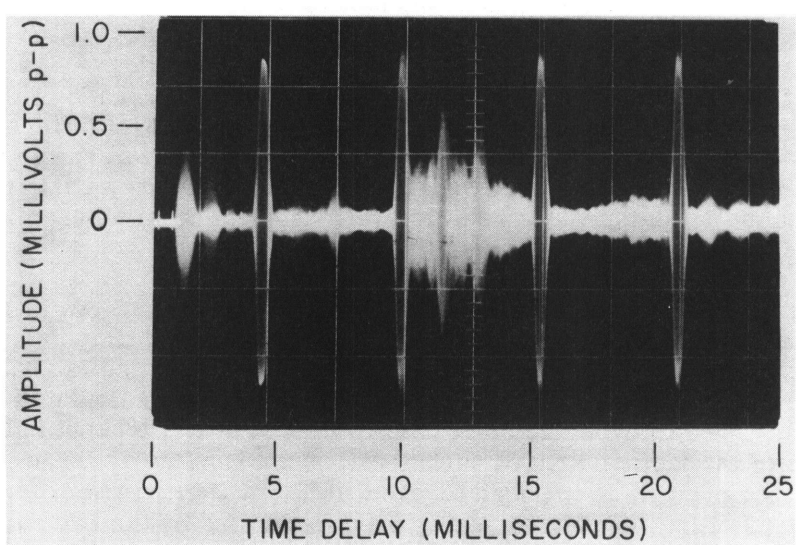

Fig. 18 - Observed backscatter (Case 3)

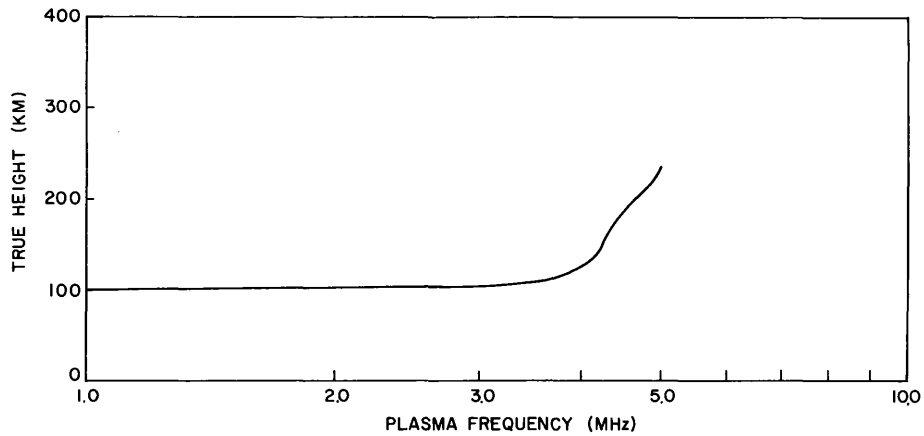

Fig. 19 - Measured ionospheric profile (Case 3)

18 msec. The geographical coverage along the 192-degree azimuth begins midway between the southern tip of Florida and Cuba and ends 250 naut mi beyond Cuba.

The backscatter profile computed for this ray trace for an isotropic earth-scatter model is shown in Fig. 21. The match of computed and measured curves at time delays after 12 msec is extremely good. The discrepancy in the position of the major peak is about 0.3 msec. The absence of any computed backscatter voltage between 9.5 and 11.4 msec is attributed to an insufficient extent of the ionospheric *E* layer in the ionospheric profile used for analysis. This circumstance is not surprising, since there was a time lapse of 40 minutes between the events of photographing the backscatter and recording the ionosonde trace. This was sufficient time to allow a significant change in the electron density profile. A more likely cause of this discrepancy, however, is the presence of sporadic *E*-layer ionization in the ray-path transit of the *E* layer but not in the vicinity of the sounder. The sporadic-*E* ionization would, in effect, result in higher *E*-layer plasma frequencies, which would allow radar backscatter return at the shorter time delays.

The use of the VRB earth-scatter model caused a small increase of the amplitude in the null at 12.7 msec, as shown in Fig. 22. The lack of substantial difference between the two computed backscatter profiles is attributed to the small difference in incidence angles of rays with the earth's surface. Under such circumstances an angular-dependent ground scatter model would produce results little different from an angular-independent model.

The ESSA ray trace for the same ionospheric conditions is shown in Fig. 23. In comparison with the NRL ray trace the initial ground range and time delay are again longer by about 3.5%. The computed backscatter for this ray trace is shown in Fig. 24. There was virtually no difference between this profile and that calculated for a roughness parameter of 15. The fit beyond 12 msec is still good, but again about half the profile is unfilled because of the lack of rays of sufficiently short time delay. The single peak in the ESSA simulated profile, as opposed to the double-peak structure of the NRL profile, is caused by the inherent differences in ray paths predicted by the two ray-trace programs. The NRL ray trace seemed to produce the backscatter profile in best agreement with the measured profile, and the isotropic earth-scatter model produced the best NRL backscatter simulation.

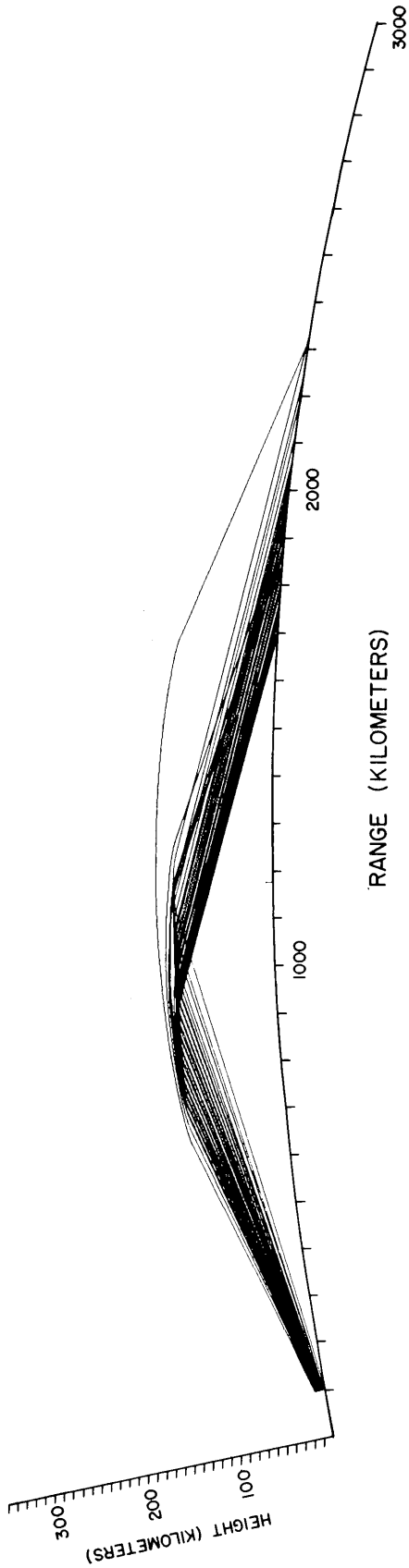

Fig. 20 - NRL ray trace (Case 3)

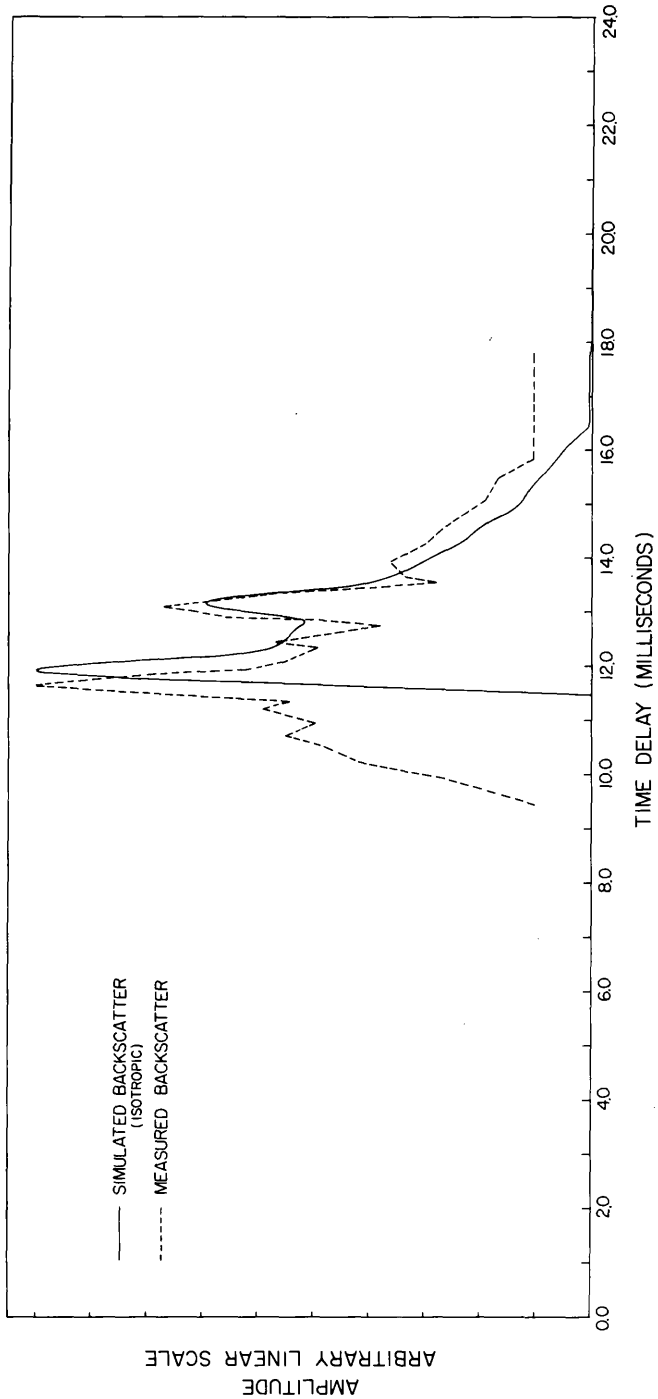

Fig. 21 - Backscatter comparison using the NRL ray trace and the isotropic earth-scatter model (Case 3). The ground range is obtained by the conversion 1 msec ≈ 150 km.

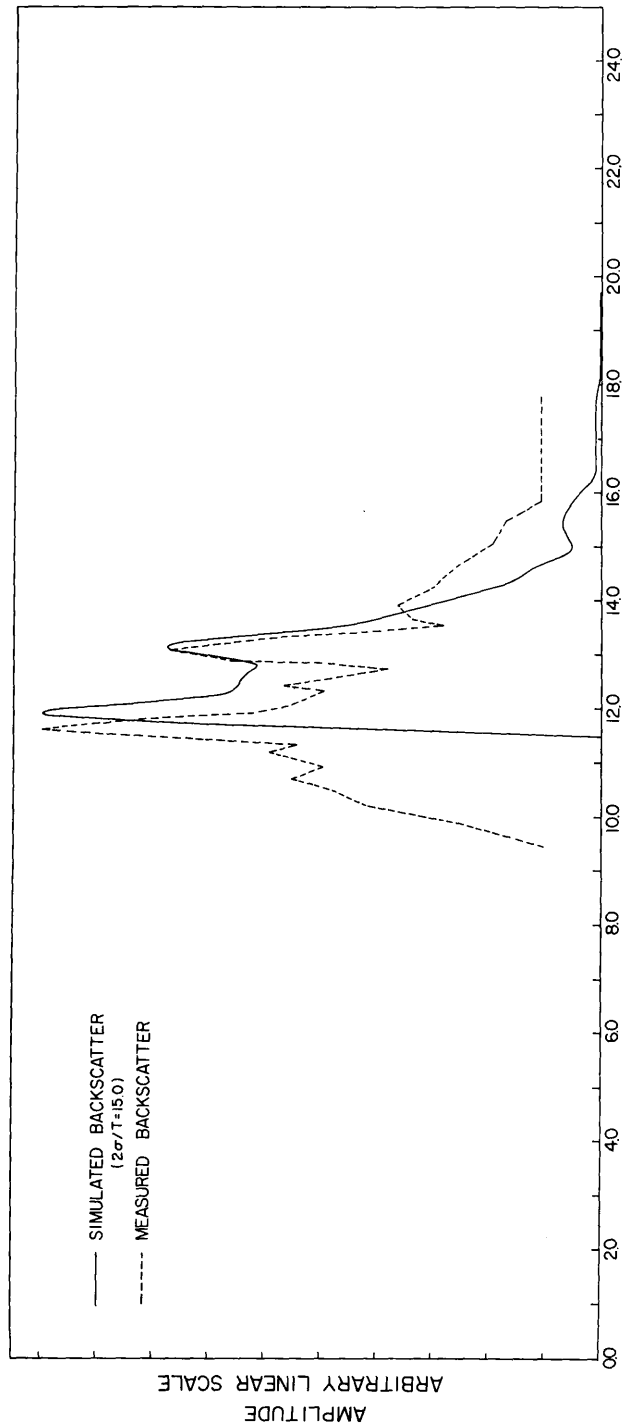

Fig. 22 - Backscatter comparison using the NRL ray trace and the VRB earth-scatter model (Case 3). The ground range is obtained by the conversion 1 msec ≈ 150 km.

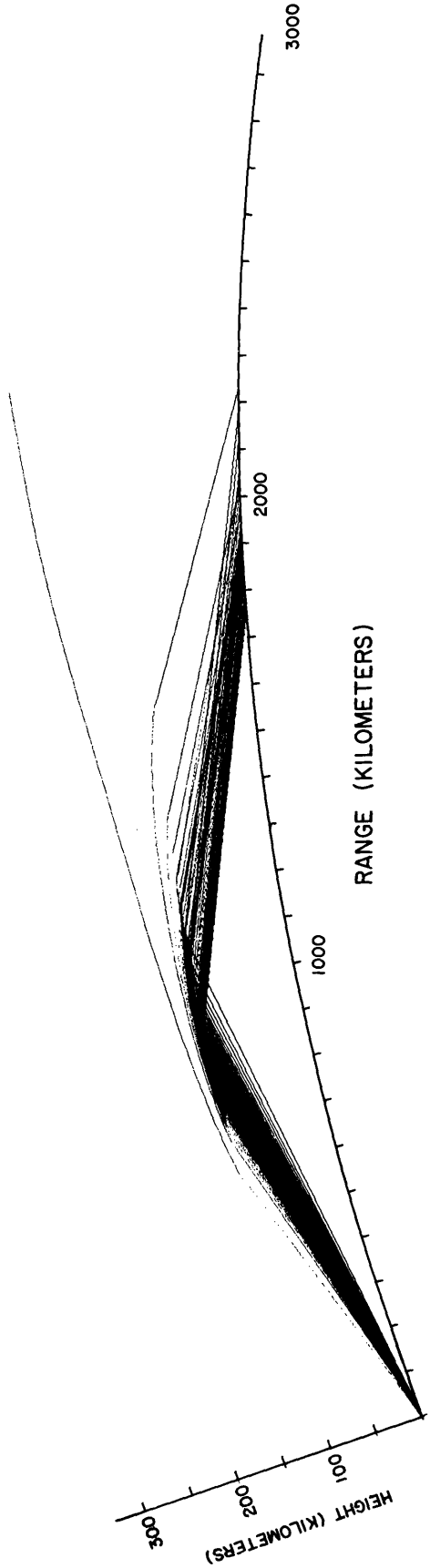

Fig. 23 - ESSA ray trace (Case 3)

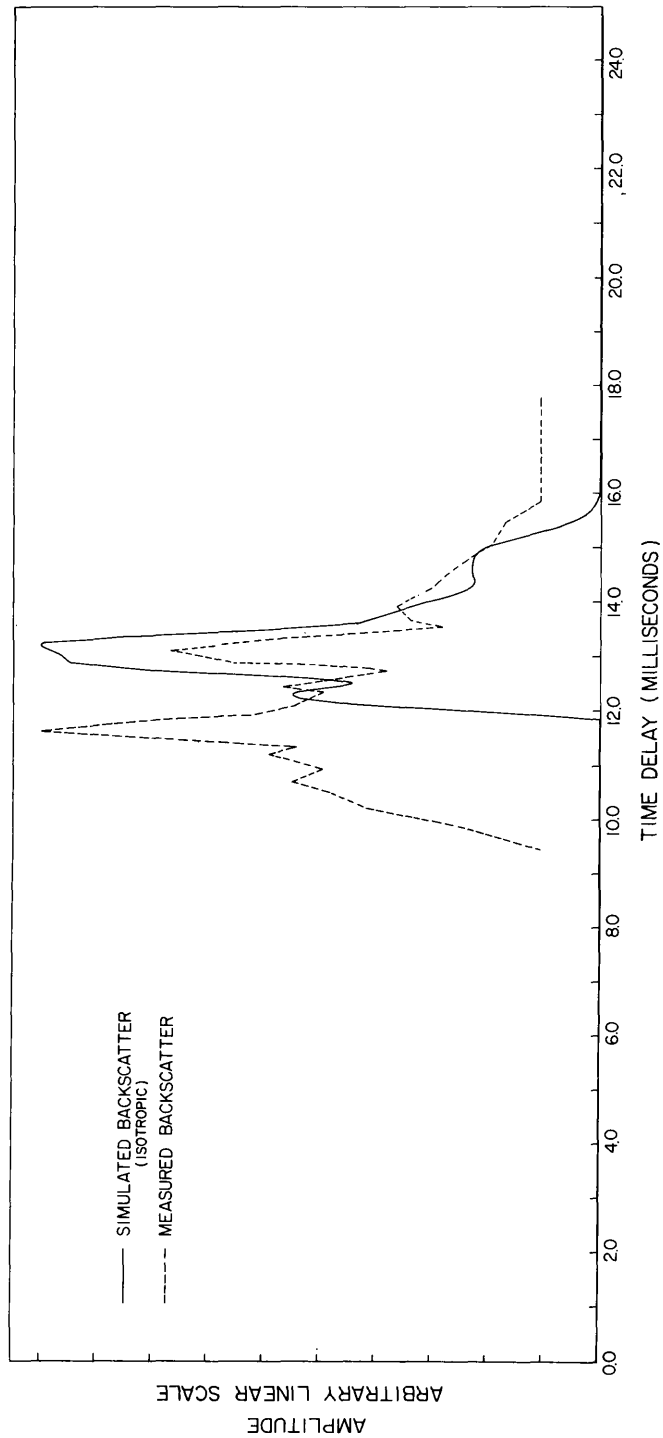

Fig. 24 - Backscatter comparison using the ESSA ray trace and the isotropic earth-scatter model (Case 3). The ground range is obtained by the conversion 1 msec ≈ 150 km.

EFFECTS OF ABSORPTION AND ANTENNA PATTERN ON BACKSCATTER

A study was conducted on the effects of absorption and antenna pattern on the backscatter profile. Four profiles, corresponding to the four possible combinations of absence or presence of either quantity were generated for each of two different ray traces based on model ionospheres. A Chapman model ionosphere (Fig. 25) was used for generating the first set of backscatter profiles. The model parameters were (a) a 300-km maximum layer height, (b) an 8.0-MHz equatorial critical frequency, and (c) a 26-km scale height.

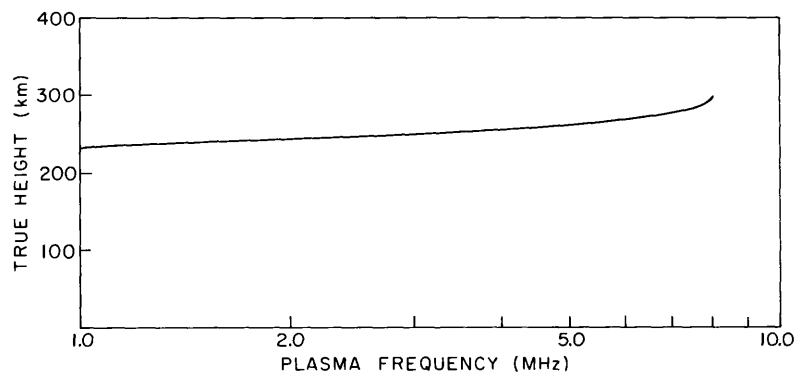

Fig. 25 - Chapman model ionospheric profile

The corresponding ray traces with and without antenna pattern are shown in Figs. 26 and 27, respectively, for a transmitter frequency of 18.036 MHz. Because of the very dense ionospheric layer, rays having up to 20-degree takeoff angles contributed to the backscatter. Three distinct antenna pattern lobes are clearly visible in Fig. 26. The upward bending of the low-angle rays at about 200 km altitude is the plotting distortion mentioned earlier. The simulated backscatter profile for no absorption or antenna pattern is shown in Fig. 28 for the isotropic and the VRB earth-scatter models. As noted previously, the VRB model with a roughness parameter of 15 yields larger amplitudes at later delay times than does the isotropic model.

The effects of absorption upon the profile are seen in Fig. 29, in which to keep the major profile peak normalized to the same height the ordinate scale is changed relative to that of Fig. 28. Here a sunspot number of 0 was used, denoting a period of minimum solar activity. The solar Greenwich hour angle (G.H.A.) and declination were 65.9 and +18.4 degrees respectively. The overall profile is similar to Fig. 28; however, the amplitudes at later time delays are relatively smaller because the contributing rays spent more time in the absorbing medium. The relative change in the maximum amplitude (the major profile peak) upon introduction of the absorption mechanism was 0.50 and 0.49 for the isotropic and VRB earth-scatter models respectively.

The relative effect of antenna pattern on the backscatter profile (Fig. 30) is to introduce nulls and peaks in that portion of the profile which was previously structureless (Fig. 28). Because of the almost mirrorlike reflection of the rays from the Chapman layer, the maxima and minima in the antenna pattern and in the backscatter profile correspond, with the low-angle lobe of the antenna pattern responsible for the peak near 22 msec. To make meaningful observations of simulated backscatter amplitude changes when changing from an isotropic to real antenna pattern, it was made certain that the

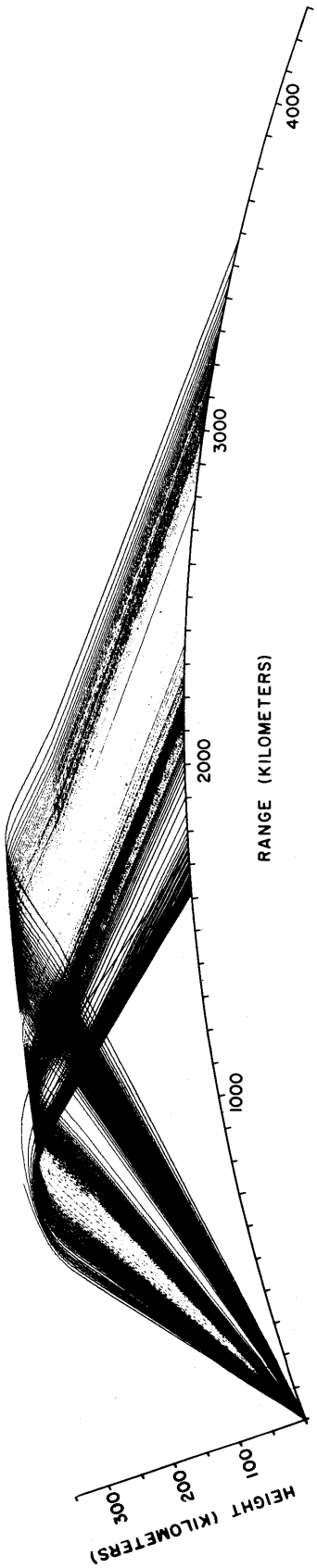

Fig. 26 – Ray trace with antenna pattern for Chapman profile

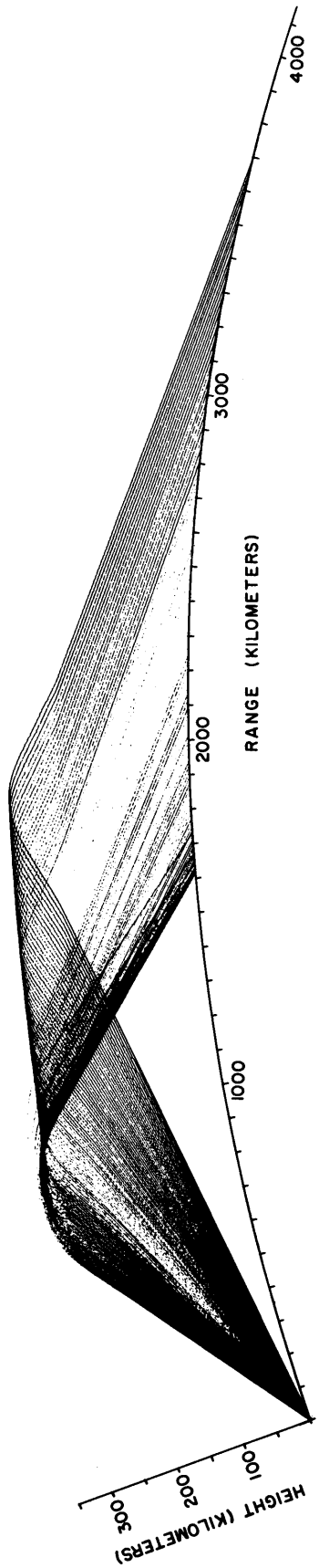

Fig. 27 – Ray trace without antenna pattern for Chapman profile. (Some of the rays near the center of the ray trace did not reproduce properly in the printing of this figure.)

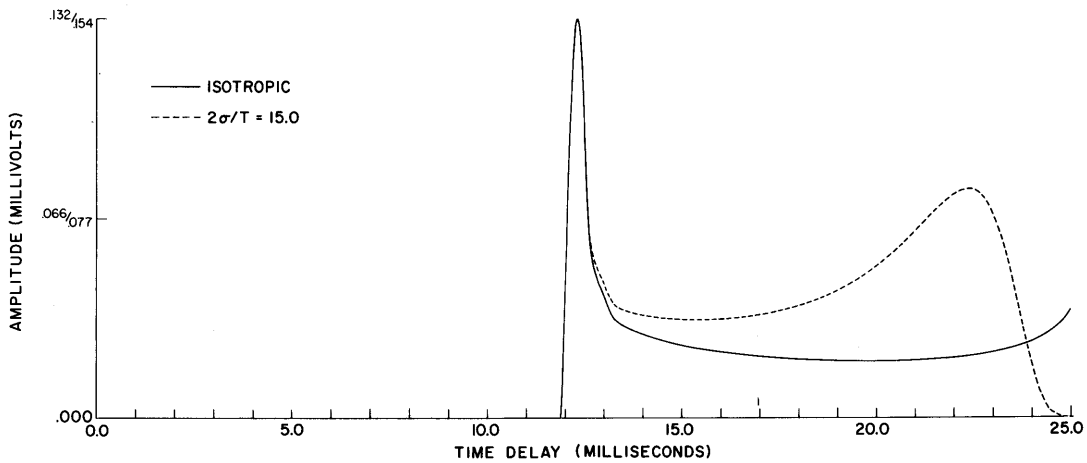

Fig. 28 - Simulated Chapman backscatter without absorption or antenna pattern for the isotropic (left-hand ordinate numbers) and the VRB (right-hand ordinate numbers) earth-scatter models

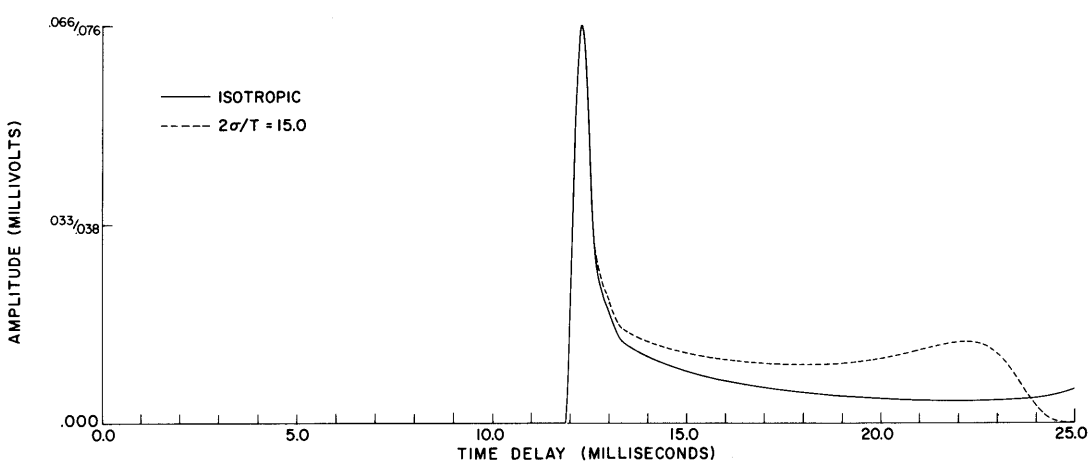

Fig. 29 - Simulated Chapman backscatter with absorption but without antenna pattern

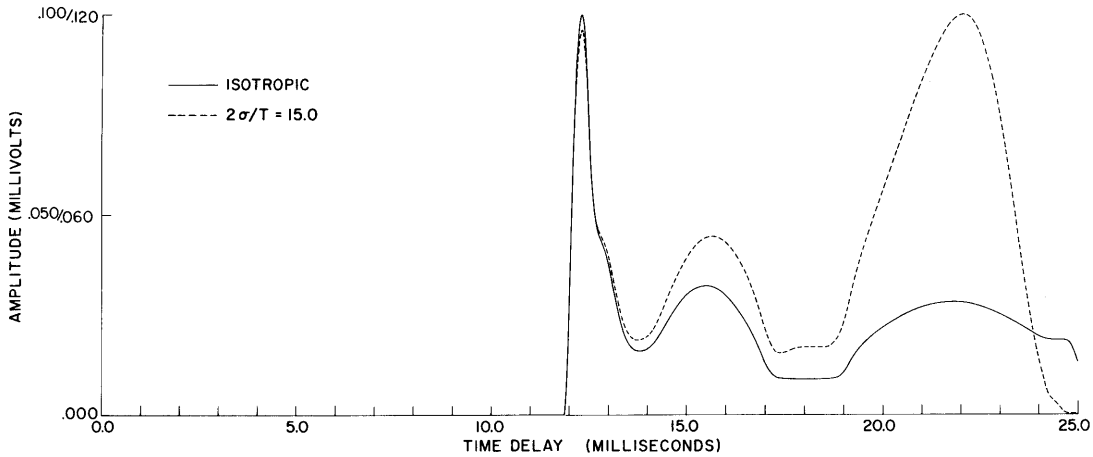

Fig. 30 - Simulated Chapman backscatter with antenna pattern but without absorption

backscatter ordinate scales represented equal total power radiated by both kinds of antennas within the total angular spread of rays. Since the program does not automatically accomplish this, the ordinate scale markers for the profiles generated with an isotropic antenna pattern were multiplied by a factor of $\sqrt{P_2/P_1}$, where P_2 is the total power carried along the rays generated according to the real antenna pattern and P_1 is the total power carried along the rays generated according to the isotropic antenna pattern. The change in amplitudes of the absolute maximum of the profile, in going from the isotropic to the real antenna pattern, were 0.758 and 0.779 for the isotropic and VRB earth-scatter models. The lower power density of the high-angle antenna pattern lobe is probably responsible for this decrease in major peak amplitude.

The effect of the addition of absorption is shown in Fig. 31. Again, as in Fig. 29, the amplitudes at larger time delays are suppressed with respect to the amplitude of the major profile peak; however, the profile structure remains qualitatively the same as for antenna pattern alone (Fig. 30). In this case the addition of absorption caused the

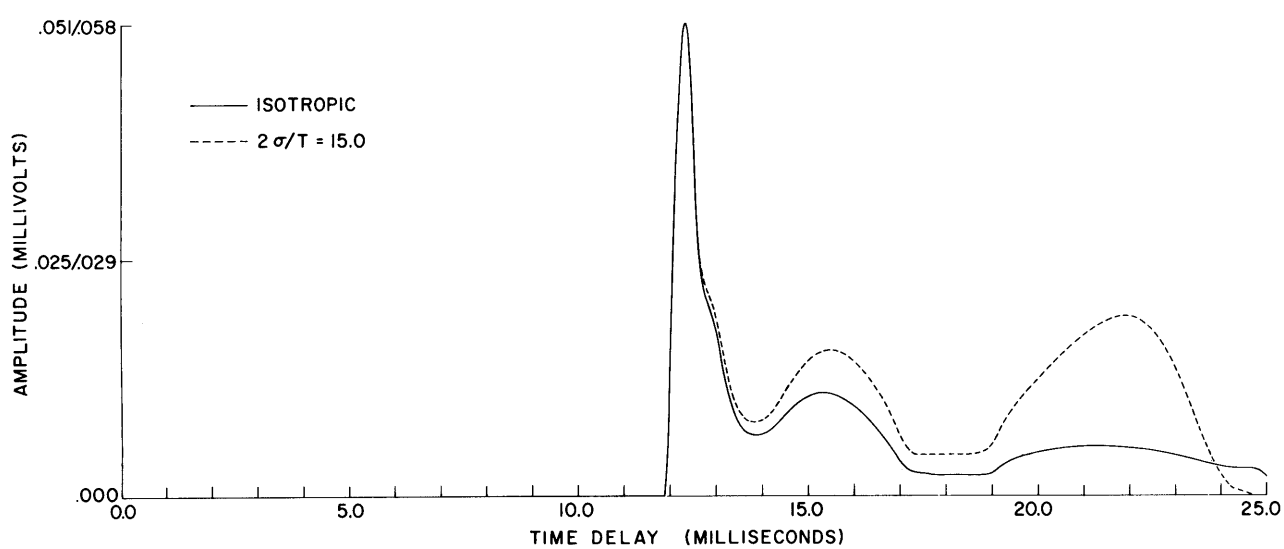

Fig. 31 - Simulated Chapman backscatter with antenna pattern and absorption

amplitude of the major peak to decrease by an additional factor of 0.51 and 0.48 for the isotropic and VRB earth-scatter model respectively, and the ordinate scales of Fig. 31 are expanded accordingly from those of Fig. 30. Additional backscatter profiles were computed for larger values of sunspot number. The effects on the major peak of the backscatter profile are given in Table 1.

Table 1
Effect of the Sunspot Number on the Reduction of the Major Peak Amplitude with the Addition of Absorption

Sunspot Number	Reduction Factor		
	Isotropic Model	VRB Model	Average
0	0.51	0.48	0.50
10	—	—	0.49
100	—	—	0.39

The effect of smaller roughness parameters of the backscatter profile is shown in Fig. 32. As a smoother surface is approached (smaller $2\sigma/T$) the greater-time-delay amplitudes are increasingly suppressed until only the major peak, near 12.2 msec, appears. A roughness parameter of 7 increases the major peak somewhat over that previously obtained, as seen by comparing the ordinate numbers, but decreasing the parameter further to 1 causes a drastic decrease in the amplitude of the peak.

A parabolic model ionospheric true height profile, shown in Fig. 33, was used to generate a second ray trace for absorption and antenna-pattern studies. The model parameters were (a) a 300-km maximum layer height; (b) a 100-km minimum layer height; and (c) a 6.0-MHz critical frequency.

The ray traces generated at 18.036 MHz with and without antenna pattern are shown in Figs. 34 and 35. In comparison with the former example, this ray trace lacks strong refraction regions, so that some high-angle and low-angle rays have similar ground ranges but different group paths. This phenomenon makes it somewhat more difficult to predict what effect the antenna pattern alone will have on the backscatter but corresponds more closely to actual conditions. Only two antenna lobes are present because of the ray penetration through the ionosphere at higher angles.

The computed backscatter for no absorption or antenna pattern is shown in Fig. 36 for the isotropic and the VRB earth-scatter models. The major backscatter peak arises from the intense illumination at a ground range of 2630 km.

The introduction of absorption (sunspot number 0, G.H.A. 65.92 degrees, declination +18.40 degrees) caused a reduction in major peak amplitude by a factor of 0.23, as seen from the ordinate numbers on Fig. 37. The larger absorption observed here than for the Chapman example under similar conditions is attributed largely to the later occurrence of the backscatter peak; this circumstance implies a longer path for the rays in the absorbing medium.

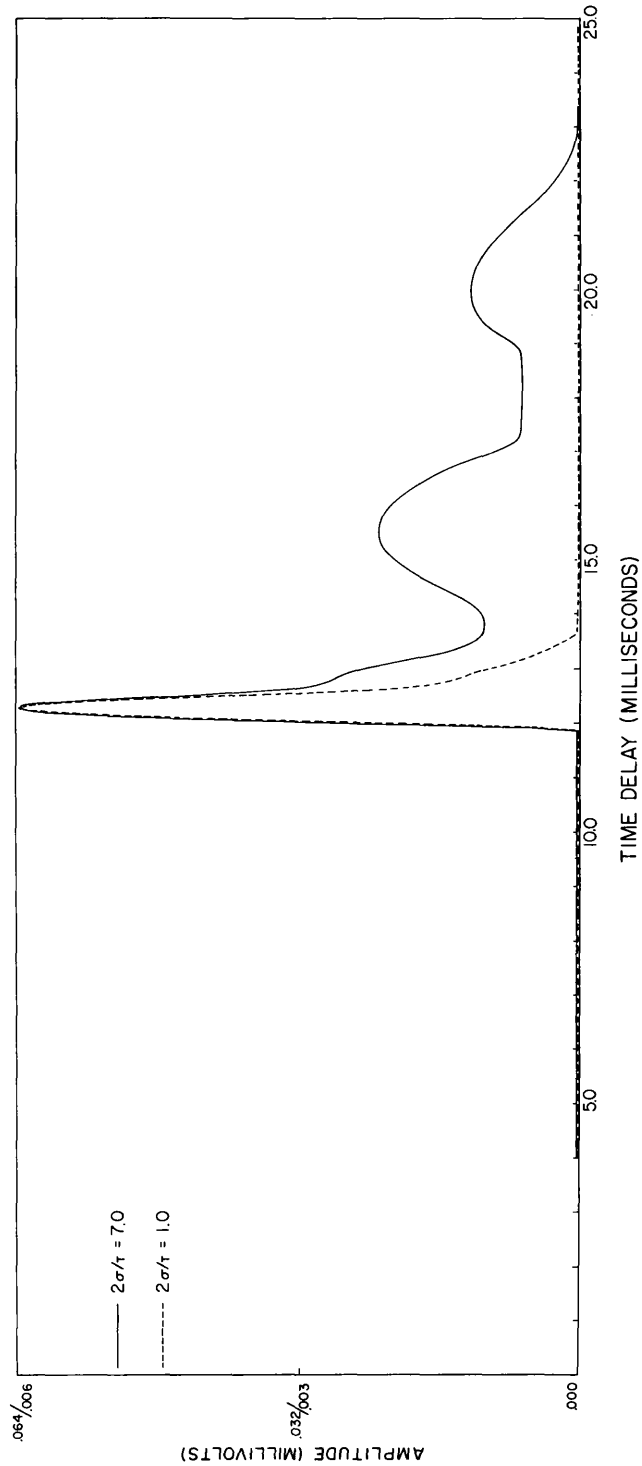

Fig. 32 - Simulated Chapman backscatter with antenna pattern and absorption for roughness parameters of 7 and 1

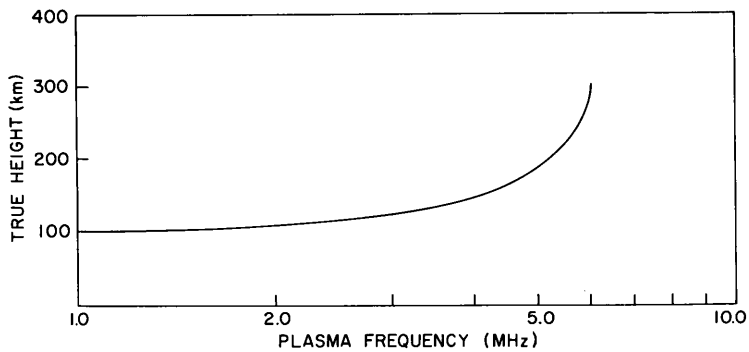

Fig. 33 - Parabolic model ionospheric profile

Introducing the antenna pattern with no absorption modified the computed backscatter profile as shown in Fig. 38. The reduction of the major peak amplitude by a factor of about 0.6 is a consequence of the first antenna pattern null reducing the illumination intensity at time delays of about 18.5 msec.

The addition of absorption, as shown on Fig. 39, again decreases the major backscatter peak amplitude by an additional factor of 0.23. The small relative change in profile shape indicates that most important ray paths spend about the same amount of time in the absorbing medium.

SUMMARY AND CONCLUSIONS

Comparison of the NRL and ESSA Ray-Trace Programs

The NRL and ESSA ray traces are usually consistent in group path and ground range within 9%, provided that overshoot has been avoided in the NRL quadratic interpolation between tabular values of the ionospheric electron-density profile. The ESSA program avoids this overshoot by using a cubic interpolation which forces continuity of the first derivative at all points on the profile. The ESSA method of interpolation will eventually be incorporated into the NRL program. Usually, but not consistently, the ESSA ray trace predicts longer ray paths.

Backscatter profiles generated from the NRL backscatter synthesis routine and the NRL and ESSA ray traces, using isotropic and nonisotropic models of diffuse scattering, were compared to actual measured profiles for three cases. A tabular input was used to describe the concurrent ionospheric electron density profile. The effects of antenna pattern and D-layer absorption on power transmission were included in the simulation. Only relative amplitudes are considered in this report, and the amplitudes have been scaled so that the maximum amplitudes of the simulated and measured profiles coincide. A summary of the findings of the three case studies is as follows.

Case 1 — In terms of quality of the overall match to the measured backscatter profile, the NRL and ESSA ray-trace simulations give equally good results. The best agreement between the NRL simulation and the measured profile was obtained using the Beckmann very-rough-surface (VRB) scattering model with roughness parameter $2\sigma/T$ = 15. It is somewhat questionable whether the isotropic or VRB earth-scatter model gives better results for the ESSA simulation.

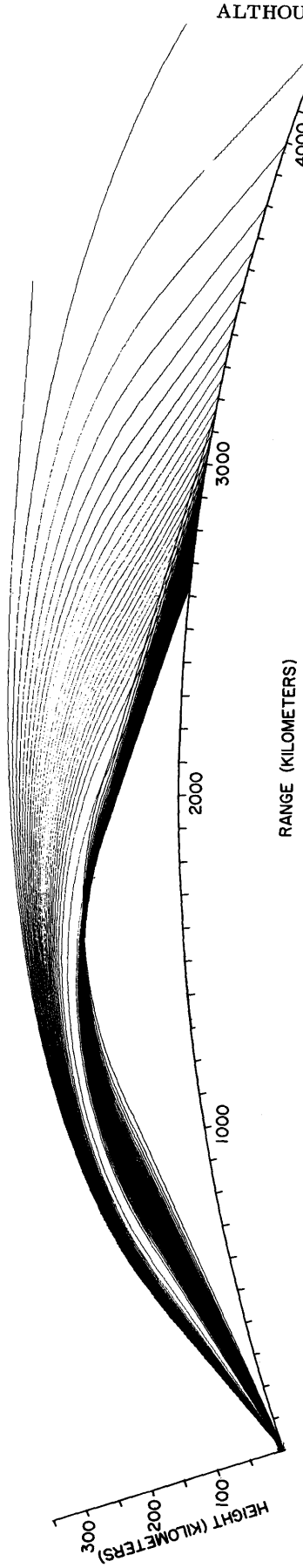

Fig. 34 - Ray trace with antenna pattern for parabolic profile

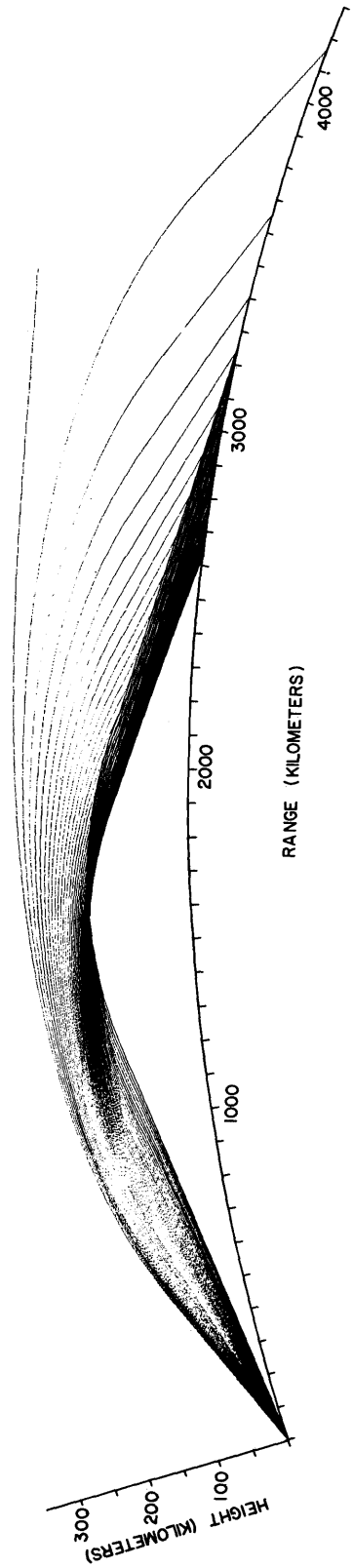

Fig. 35 - Ray trace without antenna pattern for parabolic profile

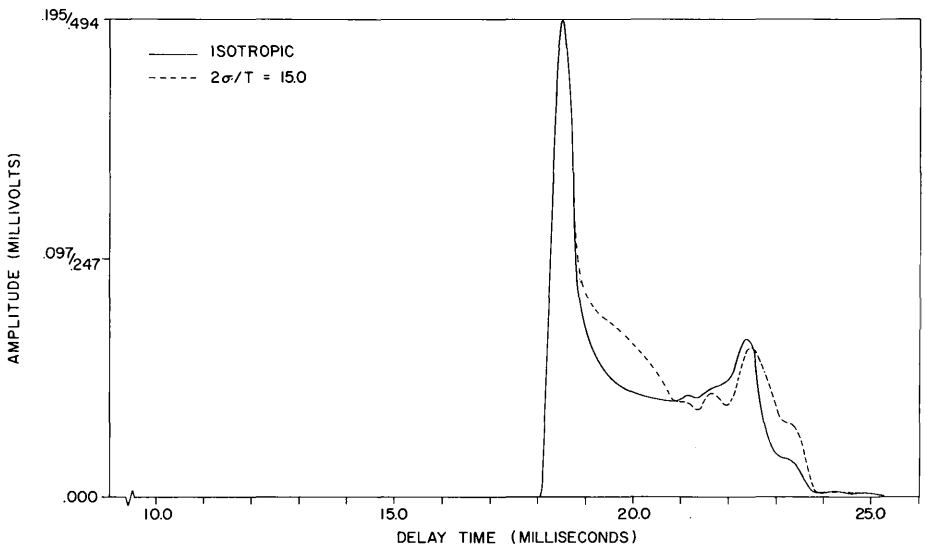

Fig. 36 - Simulated parabolic backscatter without absorption or antenna pattern

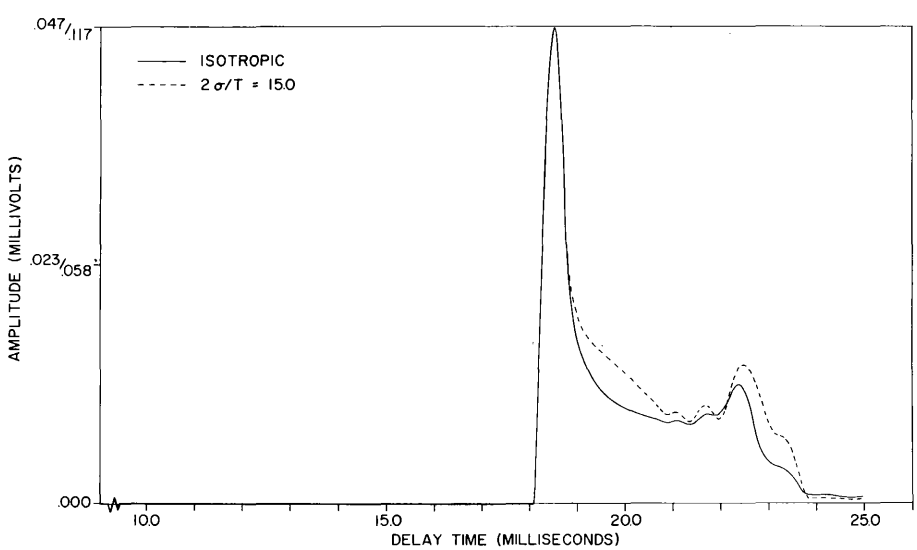

Fig. 37 - Simulated parabolic backscatter with absorption but without antenna pattern

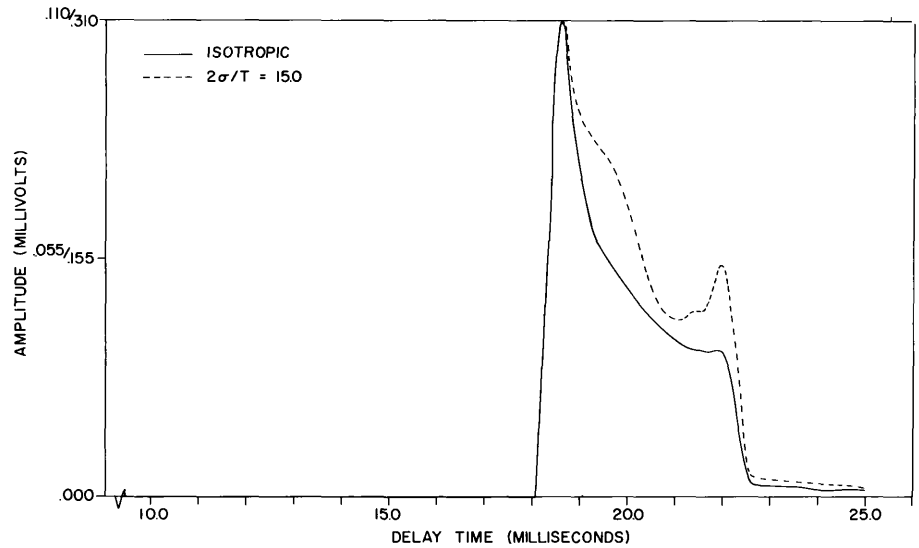

Fig. 38 - Simulated parabolic backscatter with antenna pattern but without absorption

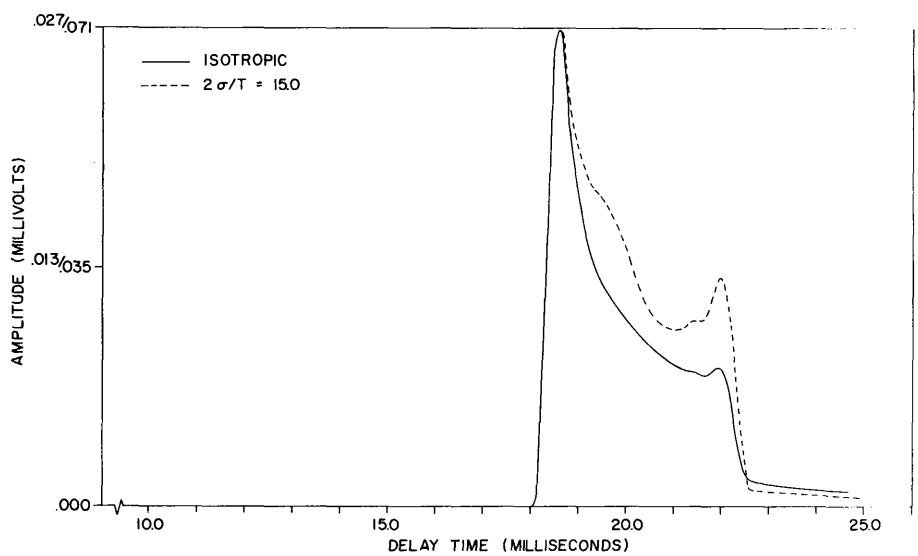

Fig. 39 - Simulated parabolic backscatter with antenna pattern and absorption

Case 2 — Again both ray-trace programs seemed to give equally good simulations to the measured backscatter using the VRB earth-scatter model. Less satisfactory results were obtained using the isotropic earth-scatter model, but differences were smaller in the ESSA simulation.

Case 3 — The NRL simulation with the isotropic earth-scatter model was the best match to the measured backscatter profile; however, the VRB scattering model did not give substantially different results. There was virtually no difference in the ESSA simulated backscatter profiles for either scattering model. The small differences produced by the two different scattering models in this case are attributed to the small angular spread of the rays incident on the earth's surface. The existence of backscatter between 9 and 11.5 msec in the measured profile but not in the simulated profile is likely to have been caused by the existence of sporadic-*E* ionization in the mid-propagation-path region but not in the vicinity of the sounder. The rather large time lapse between the measurement of the backscatter and the ionosonde trace, as well as the season and time of day (midsummer, late morning), strongly support the possibility of sporadic-*E* influence. Similar changes in the ionosphere over periods of a few minutes are sometimes experienced even in the absence of sporadic-*E* ionization, especially at dawn and dusk.

With the few backscatter comparisons studied in detail so far, and with the usually similar predictions of both ray-trace programs, it has not yet been possible to determine whether or not one ray trace consistently produces better results than the other. Similarly, a larger body of data must be examined before a preference can be established for either scattering model; however, it has been found that roughness parameters less than 1 or greater than 30 are usually unsatisfactory. The quality of the match between simulated and measured backscatter profiles for the three examples presented is considered to be good considering (a) the time difference between measured backscatter data and available ionogram data, (b) the scarcity of sounder stations along the propagation path, and (c) the uncertainty in how to model the diffuse scattering of HF electromagnetic energy by the earth's surface effectively. The recent closing down of many ionospheric sounder stations has made the prospect of getting ionograms descriptive of mid-propagation-path ionospheric conditions much poorer.

Although much research has been carried out by others in the field of rough-surface scattering of electromagnetic energy, many of the resultant scattering descriptions are so mathematically formal as to make their application to the programs described here extremely difficult if practicable at all. No studies have yet been made with this program using the Beckmann formulation for scattering from very slightly rough surfaces.

Antenna Pattern and Absorption

The effect of the antenna pattern on backscatter profiles, for an almost mirrorlike ionosphere, is to introduce peaks and troughs with one-to-one correspondence to the peaks and troughs of the antenna pattern. However, for more complex ionospheres having appreciable focusing effects, and corresponding more closely to reality, it is difficult to predict the effect the antenna pattern will have on the backscatter structure. Only after a simulation is performed with and without antenna pattern for the ionosphere under consideration will the effect of the antenna pattern on the backscatter be obvious.

Typically, the effect of absorption is to reduce the overall amplitude of the backscatter profile, with slightly greater effect at longer time delays.

Plans for Future Study

The backscatter simulation technique, in conjunction with the scattering and absorption models, will be applied in the future to a much larger body of data, obtained with different types of terrain, to attempt to determine the fraction of incident power σ^0 that is returned to the radar. It is anticipated that σ^0 will be a function of the terrain itself, due to its surface roughness characteristics, as well as a function of the incidence angles of the rays responsible for the major part of the backscatter return. Also, a large body of simultaneously measured backscatter and ionospheric sounder data closely spaced in time will be analyzed, to assess the ability of the method to handle accurately short-term variations (of the order of minutes) in backscatter due to the associated ionospheric changes.

The addition of another subroutine to those described in this report will be used for predicting illumination density on the earth using a comparison of simulated and measured earth backscatter as a diagnostic method for ascertaining that coverage. Attempts are already in progress to simulate earth backscatter using magnetic-field-dependent ray tracing. This technique will clarify the significance of the errors inherent in the simpler approach.

Implementation of ionospheric-tilt models into the ray-trace/backscatter simulation routines is being considered as a first step toward a two-dimensional treatment of the ionospheric electron density profile. It is evident, however, that sophisticated two-dimensional, birefringent ionosphere ray tracing becomes almost prohibitively expensive at present computer speeds, when used to calculate the hundreds of rays necessary to simulate accurately backscatter profiles for a large sample of data.

REFERENCES

1. Davis, J.R., Harding, M.E., Willis, J.W., and Utley, F.H., "Applications of Computer-Aided Ionospheric Ray Tracing Techniques to the Analysis of Over-the-Horizon Radar Signatures From Launch-Phase Rockets," NRL Report 6731 (Secret Report, Unclassified Title), July 30, 1968

2. Jones, R.M., "A Three-Dimensional Ray Tracing Computer Program," ESSA Technical Report IER 17-ITSA 17, December 1966; also, "Modifications to the Three-Dimensional Ray Tracing Program Described in IER 17-ITSA 17," Vol. I, December 1967

3. Haselgrove, J., In "The Physics of the Ionosphere, Report of the Physical Society Conference," Cambridge, 1954, London, The Physical Society, pp. 355-364, 1954

4. Haydon, G.W., and Lucas, D.L., "Predicting Statistical Performance Indexes for High Frequency Ionospheric Telecommunications Systems," ESSA Technical Report IER 1-ITSA 1, Aug. 1966

5. Beckmann, P., and Spizzichino, A., "The Scattering of Electromagnetic Waves from Rough Surfaces," New York:Pergamon, 1963, pp. 88-89

Security Classification

DOCUMENT CONTROL DATA - R & D

(Security classification of title, body of abstract and indexing annotation must be entered when the overall report is classified)

1. ORIGINATING ACTIVITY *(Corporate author)* Naval Research Laboratory Washington, D.C. 20390	2a. REPORT SECURITY CLASSIFICATION Unclassified 2b. GROUP

3. REPORT TITLE

COMPUTER SIMULATION OF STRUCTURAL DETAILS OF HIGH-FREQUENCY OVER-THE-HORIZON EARTH BACKSCATTER

4. DESCRIPTIVE NOTES *(Type of report and inclusive dates)*

An interim report on a continuing NRL Problem.

5. AUTHOR(S) *(First name, middle initial, last name)*

E.L. Althouse, J.R. Davis, and P.E.V. Shannon

6. REPORT DATE November 24, 1969	7a. TOTAL NO. OF PAGES 42	7b. NO. OF REFS 5
8a. CONTRACT OR GRANT NO. NRL Problem R02-23 b. PROJECT NO. RF 05-151-402-4007 c. MIPR FB 2835-9-916 d.	9a. ORIGINATOR'S REPORT NUMBER(S) NRL Report 6960 9b. OTHER REPORT NO(S) *(Any other numbers that may be assigned this report)*	

10. DISTRIBUTION STATEMENT

This document has been approved for public release and sale; its distribution is unlimited.

11. SUPPLEMENTARY NOTES	12. SPONSORING MILITARY ACTIVITY Department of the Navy (Office of Naval Research), Washington, D.C. 20360 and Department of the Air Force (Rome Air Development Center). Griffiss Air Force Base, New York 13440

13. ABSTRACT

A computer program was developed which simulates high-frequency radar backscatter profiles (giving the amplitude as a function of time delay) from previously computed ray trajectories. The ray trajectories were computed from two different ray-tracing programs; both programs use tabular input descriptions of the antenna pattern and ionospheric electron density profile. One ray-trace program, written at NRL, is a two-dimensional program which generates refraction of the ray trajectories in the ionosphere by applying Snell's law at the boundary of each incremental slab in a uniformly spherically stratified, earth-concentric ionosphere with changing index of refraction. The second, called the ESSA ray-trace program, was written at The Institute for Telecommunication Sciences and Aeronomy, Boulder, Colorado, but was modified at NRL to include the effects of antenna pattern. The ESSA program generates the ray trajectories by performing a three-dimensional, error-checking numerical integration of the six differential Haselgrove equations.

The backscatter profiles which result from the ray trajectories in conjunction with the backscatter synthesis program were compared to actual measured profiles for three cases. The purposes of comparisons between simulated and measured backscatter profiles are: (a) to test the hypothesis that ray trajectories can be predicted reasonably accurately for an HF radar using reduced ionogram data from an appropriately located sounder, (b) to observe the consequences of differences inherent in the two methods of ray tracing, and (c) to investigate the relative validity of various earth backscatter models having dependence on surface roughness and on the elevation angles of the arriving and returning rays.

(OVER)

DD FORM 1 NOV 65 1473 (PAGE 1)

S/N 0101-807-6801

Security Classification

Security Classification

14. KEY WORDS	LINK A ROLE	LINK A WT	LINK B ROLE	LINK B WT	LINK C ROLE	LINK C WT
Radar						
High frequencies						
Over-the-horizon radar						
Earth backscatter						
Backscatter						
Ionosphere						
Electron density profiles						
Computer programs						
Ray tracing						
Simulation						

An analysis was performed for two different model ionospheric electron density profiles to assess the effects of antenna pattern and D-layer absorption on the backscatter profile.

Direct comparison of the ray paths in the three cases studied showed that NRL and ESSA ray traces are usually consistent in group path and ground range within 9%, with the ESSA ray trace predicting longer ray paths in most instances. Good agreement was obtained between the simulated and measured backscatter profiles in two of the three cases for both ray-trace programs, and the hypothesis in (a) was strongly supported.

DD FORM 1 NOV 65 1473 (BACK)
(PAGE 2)